The Thesis Committee for Jimi Kim
Certifies that this is the approved version of the following thesis

Disruption of Mitochondrial Folate Transporter Gene (*Slc25a32*) Induces Embryonic Lethality and Neural Tube Defects in Mice

APPROVED BY
SUPERVISING COMMITTEE:

Supervisor:

Richard H Finnell

Molly S Bray

Disruption of Mitochondrial Folate Transporter Gene (*Slc25a32*) Induces Embryonic Lethality and Neural Tube Defects in Mice

by

Jimi Kim

Thesis

Presented to the Faculty of the Graduate School of

The University of Texas at Austin

in Partial Fulfillment

of the Requirements

for the Degree of

Master of Arts

The University of Texas at Austin

August 2017

Disruption of Mitochondrial Folate Transporter Gene (*Slc25a32*) Induces Embryonic Lethality and Neural Tube Defects in Mice

Jimi Kim, M.A.

The University of Texas at Austin, 2017

Supervisor: Richard H Finnell

Neural tube defects (NTDs) represent the most common class of structural congenital malformations in humans. While periconceptional supplementation with folic acid (FA) may prevent up to 70% of NTDs, a well-developed intervention strategy is required to address the remaining 30±% of NTDs that are non-responsive to folate intervention. During pregnancy, FA provides essential one carbon (1C) units for nucleotide and methyl group biosynthesis through folate mediated 1C metabolism to proper neural tube closure (NTC). Mitochondrial folate transporter (MFT, encoded by the SLC25A32 gene) transports tetrahydrofolate (THF), the bioactive form of FA, into mitochondria. We characterized a novel folate mitochondrial transport mouse model by inactivating the *Slc25a32* gene. Inactivation of the *Slc25a32* gene resulted in embryo-fetal lethality, as the *Slc25a32*$^{gt/gt}$ fetuses die *in utero* by E12.5. Perturbation of the *Slc25a32* allele exhibited abnormalities of NTC, resulting in fully penetrant NTDs of exencephaly and

craniorachischisis in the *Slc25a32*$^{gt/gt}$ embryos, as well as an increased prevalence of craniofacial defects and a reduction in embryonic growth compared to the wild-type embryos. Maternal folic acid supplementation, 5-methyl-tetrahydrofolate (5-mTHF), was ineffective in reducing the prevalence of NTDs in *Slc25a32*$^{gt/gt}$ embryos. These NTDs were partially rescued by maternal supplementation with calcium formate, which is a downstream output product of the mitochondrial folate 1C pathway. This study proposed to utilize the *Slc25a32* mouse model as a novel tool for studying the function FA in the mitochondria with respect to NTC, the mechanisms that underlie the failure of NTC in the mouse model of folate-resistant NTDs.

Table of Contents

List of Tables

List of Figures

1 Introduction

Neural tube defects (NTDs) are one of the most common structural congenital malformations in humans, resulting from failed closure of the neural tube. NTDs compromise over 2,300 pregnancies each year in the United States (CDC 2004), and more than 330,000 babies born globally (Murray et al. 1998). The prevalence of NTDs ranges from 0.5 to 2 per 10,000 live births worldwide (Mitchell 2005). Neural tube closure (NTC) is the morphological process occurring in early embryogenesis that will ultimately create the adult central nervous system including the brain and spinal cord. The initiation of NTC involves the elevation of neural folds from the neural plate, ultimately fusing at the dorsal midline along the rostral-caudal embryonic axis. The process of NTC is influenced by multiple factors including nutrition, environmental factors, and genetics under a complex interaction of cellular and molecular mechanisms (Nikolopoulou et al. 2017). NTDs arise secondary to a failure of NTC and are classified as either open or closed (Copp & Greene 2012). Open NTDs include anencephaly, myelomeningocele (spina bifida), and craniorachischisis. Fetuses with anencephaly and craniorachischisis die prior to or shortly after birth. In closed NTDs, spinal lesions are covered by skin; these include lipomyelomeningocele and tethered cord.

Decades of research has shown that a deficiency of folic acid (FA), together with as-yet unknown genetic variants and additional environmental factors, contribute to the multifactorial risk of NTDs. Folate is required for multiple cellular processes, including nucleotide synthesis, DNA repair, genomic stability, mitochondrial protein synthesis, and methylation reactions, including histone methylation (Lucock 2000) (Tibbetts & Appling

2010). Over the past 20 years, a vast literature has developed studying the relationship between NTDs and the maternal periconceptional consumption of FA, which is the synthetic form of folate. The prevalence of NTDs was shown to be significantly reduced by up to 70% due to the protective effect of maternal FA supplementation (Czeizel 1998), resulting in the recommendation that pregnant women should consume at least 400 μg/day (MRC Vitamin Study Research Group 1991). However, there remain a significant number of infants born with NTDs that appear to be folate-resistant, as the periconceptional administration of FA is unable to prevent all NTDs (Copp, Stanier, and Greene 2013).

In an effort to identify just how deficiencies in folate metabolism causes NTDs, our laboratory has created genetically modified mice with homozygous deletions of critical folate transport genes including: the human proton coupled folate transporter (*Pcft*), the bidirectional reduced folate carrier 1 (*Rfc1*), and the glycosylphosphatidylinositol-anchored folate receptors (*Folr1*, *Folr2,* and *Folr4*). The monoglutamyl folates are absorbed by PCFT that is encoded by *SLC46A1* under optimum pH of 5.5 in the small intestine. Homozygous *Pcft* knockout mouse die between 50 and 60 days post-parturition, suffering from a hereditary folate malabsorption which produces macrocytic normochromic anemia and pancytopenia impaired with erythropoiesis and thrombopoiesis (Salojin et al. 2011). RFC1 encoded by *SLC19A1* also serves as a monoglutamyl folate transporter, resulting in reduced and methylated forms such as 5-methyl-THF (5-mTHF) entering into systemic circulation. Homozygous *Rfc1* knockout embryos are embryo-lethal by E9.5 (Waes et al. 2008), while homozygous knockout *Folr1* embryos exhibited embryo-lethality and folate-responsive cranial NTDs (Piedrahita et al. 1999) (Saitsu 2017).

In eukaryotes, folate 1C metabolism occurs in parallel between the cytosol and mitochondria. Reduced tetrahydrofolates (THFs) play an important role in folate 1C metabolism, as either a 1C donor or acceptor, or transporting 1C groups through reciprocal conversions (Tibbetts & Appling 2010). Folate 1C metabolism also supports *de novo* synthesis of purine, thymidylate and homocysteine re-methylation to methionine, supporting DNA replication and RNA production. Folate 1C metabolism also regulates apoptosis during cell cycle, and plays a role in the epigenetic regulation of DNA methylation (Lane & Fan 2015) (Chu & Allegra 1996) (Crider et al. 2012).

Cytoplasmic folate consisting of the monoglutamate form of THFs, are transported into mitochondria by the mitochondrial folate transporter (MFT, encoded by *SLC25A32* gene) localized in the inner mitochondria membrane (Lawrence, Hackett, and Moran 2011). Mitochondrial folate 1C metabolism is THF-dependent catabolism facilitated by mitochondrial THF derived from the cytosol (Tibbetts & Appling 2010). Mitochondrial THF carries 1C units to generate CH_2-THF from serine catalyzed by the mitochondrial enzyme serine hydroxymethyltransferase (SHMT2), producing glycine via the glycine cleavage system (GCS). CH_2-THF is oxidized to CHO-THF by mitochondrial bifunctional CH_2-THF dehydrogenase/methenyl-THF cyclohydrolase (MTHFD2, encoded by *MTHFD2* gene) or mitochondrial CH2-THF dehydrogenase (MTHFD2L, encoded by *MTHFD2L* gene). CHO-THF is a co-substrate to generate formate via the enzyme mitochondrial monofunctional 10-formyl-THF synthetase (MTHFD1L, encoded by *MTHFD1L* gene). Formate is the end product of mitochondrial folate metabolism derived from mitochondrial THF and is transported into the cytoplasm to provide 1C units

necessary for proper nucleotide biosynthesis and methylation reactions (Tibbetts & Appling 2010). At least 75% of the 1C units in cytoplasmic folate 1C metabolism are derived from the mitochondria (Pike et al. 2010), suggesting that the mitochondrial folate transport system plays a critical role in the folate 1C metabolism by transporting THF, a carrier of 1C units, in both the cytosol and mitochondria.

1.1 Folate One Carbon Metabolism

Folate is an essential B vitamin (B9) that mammalian cells cannot synthesize and must be obtained through the diet or via supplementation. For folate to be transported within the cell, it must be polyglutamylated by folylpolyglutamate synthase (FPGS), and these conjugases are reduced to generate 5,6,7,8-tetrahydrofolate (THF) by dihydrofolate reductase (DHFR). The polyglutamate form of folate must be hydrolyzed to a monoglutamate for absorption and transport. The THF is a reduced pteridine species composed of three chemical moieties; pteridine, *p*-aminobenzoic acid, and a poly-ɣ-glutamate tail, and this bioactive form transports 1C units by binding them at N5 and N10 of the pteridine and *p*-aminobenzoic acid. A pool of THF coenzymes is linked closely to the 1C units, and makes it possible for the THF to participate in various metabolic process referred to as 1C metabolism (Tibbetts & Appling 2010).

As describe in Fig. 1, folate-mediated 1C metabolism occurs in parallel between the cytosol and mitochondria in eukaryotes (Barlowe & Appling 1988a). Activated 1C units are transported by THF from donors such as serine (García-Martínez & Appling 1993), glycine (Hampson, Taylor, and Olson 1983), sarcosine (Barlowe & Appling 1988b), dimethylglycine or formate between the mitochondria and cytosol (Cybulski & Fisher

1977) (Palmieri 2013). In the cytosol, THF generates 5,10-methylene-THF (CH_2-THF) by accepting 1C of serine from glycolytic intermediates. This serine reaction is processed by cytoplasmic serine hydroxymethyltransferase (SHMT1), and its 3-carbon is conveyed to THF, producing glycine. Both serine and glycine are transported by the same amino acid carrier (García-Martínez & Appling 1993) and serve as 1C donors between the cytosol and mitochondria (Yoshida & Kikuchi 1970). Cytoplasmic CH_2-THF is a core substance for *de novo* thymidine synthesis, 5-methyl-THF (CH_3-THF) formation to homocysteine remethylation, and 5,10-methenyl-THF (CH^+-THF) conversion. CH_2-THF produces CH^+-THF by the monofunctional NAD-dependent enzyme CH_2-THF dyhydrogenase. CH^+-THF is oxidized to 10-formyl-THF (CHO-THF) for purine synthesis by CH^+-THF cyclohydrolase. CHO-THF is converted to THF and formate by the enzyme CHO-THF synthetase in an ATP-dependent manner. The reactions described above are catalyzed by methylenetetrahydrofolate dehydrogenase (MTHFD1, encoded by the *MTHFD1* gene) (MacFarlane et al. 2009), trifunctional C1-THF synthase in the cytosol. As mentioned above, CH_2-THF is reduced to CH_3-THF by 5,10-methylene-THF reductase (MTHFR), encoded by the *MTHFR* gene (Ho, Massey, and King 2013) to enter the cytosolic methyl cycle. CH_3-THF provides the methyl group to homocysteine for methionine synthesis. Methionine catalyzes S-adenosyl methionine (SAM) by methionine adenosyl transferase, which is subsequently involved in homocysteine re-methylation (Agrimi et al. 2004). Ultimately, the cytoplasmic folate-mediated 1C process is important for the *de novo* synthesis of purine and thymidylate, and for homocysteine remethylation to methionine.

Mitochondria folate-mediated 1C metabolism parallels the cytosolic pathway. The main function of mitochondria folate-mediated 1C metabolism is to supply formate to the cytosol for nucleotide biosynthesis and methylation reactions. In mitochondria folate-mediated 1C metabolism, the cytoplasmic monoglutamate form of THF is transported into mitochondria by means of the mitochondrial folate transporter (MFT, encoded by the *SLC25A32* gene) localized in the inner mitochondria membrane (Palmieri 2013) (Lawrence et al. 2011). Mitochondrial THF generates CH_2-THF by carrying 1C units from serine with SHMT2 (Pfendner & Pizer 1980), producing glycine. Unlike cytoplasmic glycine, mitochondrial glycine can transfer 1C units to THF via the GCS (Kikuchi et al. 2008) (Lamers et al. 2009). CH_2-THF is catalyzed to CH^+-THF by mitochondrial NAD-dependent CH_2-THF dehydrogenase. CH^+-THF is oxidized to CHO-THF by mitochondrial CH^+-THF cyclohydrolase. These reactions are catalyzed by mitochondrial bifunctional CH_2-THF dehydrogenase (MTHFD2, encoded by *MTHFD2* gene) (Mejia & MacKenzie 1988) or mitochondrial CH_2-THF dehydrogenase (MTHFD2L, encoded by *MTHFD2L* gene) (Shin et al. 2014). CHO-THF is a co-substrate to generate formyl methionine transfer RNA (fMet-tRNA) by CHO-THF dehydrogenase, and formate by mitochondrial CHO-THF synthetase in an ATP-dependent manner, respectively. It is catalyzed by mitochondrial monofunctional 10-formyl-THF synthetase (MTHFD1L, encoded by *MTHFD1L* gene (Prasannan et al. 2003) (Prasannan & Appling 2009) (Pike et al. 2010), monofunctional C1-THF synthase in the mitochondria. Mitochondrial formate exits to the cytoplasm and then contributes to regenerate THF and produce purines (Fig. 1).

Previous studies have demonstrated that the MFT protein encoded by *SLC25A32* gene is an exclusive THF transporter from the cytosol to mitochondria (Tibbetts & Appling 2010) (Ducker & Rabinowitz 2016). The existence of *MFT* gene was determined from a glycine auxotrophy *glyB* cell derived from Chinese hamster ovary (CHO) cells (Kao, Chasin, and Puck 1969). The *MFT* gene was identified by transduction of a retroviral human placental cDNA library into *glyB* CHO cells shown to be auxotrophic for glycine and lacking in mitochondrial folate accumulation (Kao et al. 1969) (Titus & Moran 2000). The function of MFT on embryonic development in proper closure of the neural tube in mice remains unexplored.

This study identified a link between the role of the *Slc25a32* gene and the development of NTDs. To identify the role of the mitochondrial folate transporter during embryonic development, we created a new mouse NTD model that lacks a functional *Slc25a32* gene. The disruption of the *Slc25a32* gene results in embryo-fetal lethality, and induces morphological abnormalities of NTC in the entire head region of developing mouse embryos. The inactivated *Slc25a32* embryos express completely penetrant NTDs. In this study, we hypothesize that the *Slc25a32* gene is associated with the occurrence of NTDs because it is essential for THF to participate in the mitochondrial folate 1C metabolism.

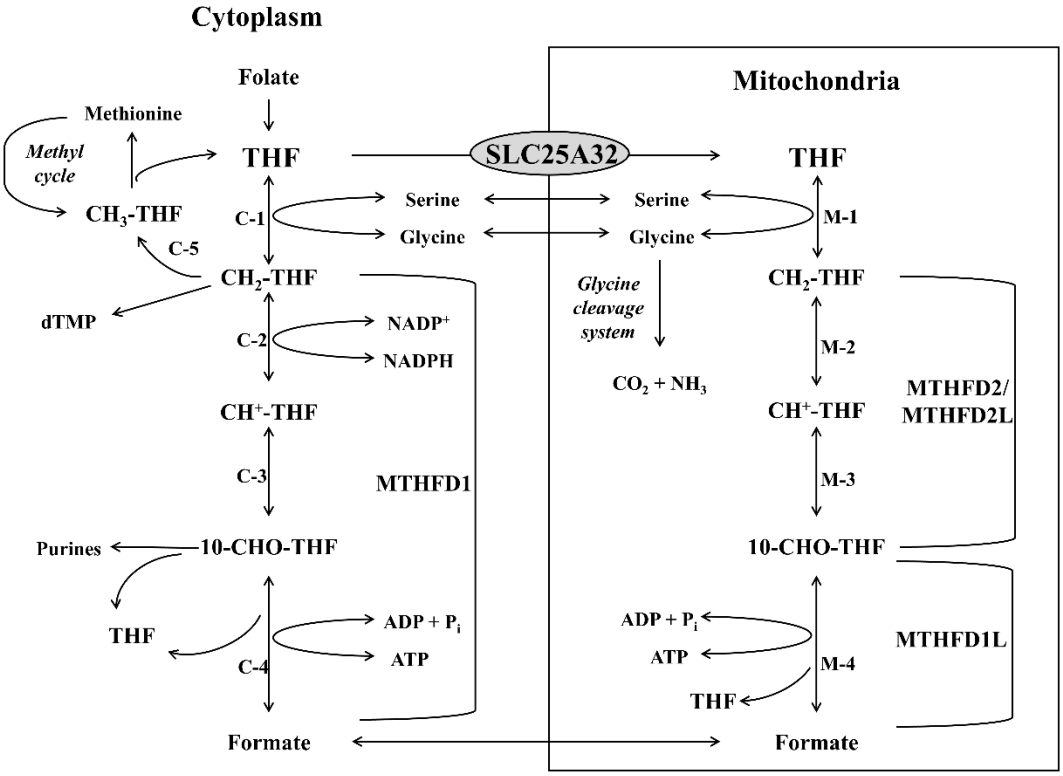

Figure 1. Folate One Carbon (1C) Metabolism

Reactions from C-1 to C-5 are in the cytoplasm and reactions from M-1 to M-4 are in the mitochondrial metabolism. Reactions C-1 and M-1, serine hydroxymethyltransferase; C-2 and M-2, 5,10-methylene-THF (CH_2-THF) dehydrogenase; C-3 and M-3, 5,10-methenyl-THF (CH^+-THF) cyclohydrolase; C-4 and M-4, 10-formyl-THF (10-CHO-THF) synthetase; C-5, 5,10-methylene-THF reductase, respectively. The reactions described above C-2, C-3, and C-4 are catalyzed by methylenetetrahydrofolate dehydrogenase (MTHFD1, encoded by the *MTHFD1* gene), trifunctional C1-THF synthase in the cytosol. In mitochondria, reactions M-2 and M-3 are catalyzed by methylenetetrahydrofolate dehydrogenase (MTHFD2 or MTHFD2L, encoded by *MTHFD2* and *MTHFD2L* genes, respectively), bifunctional C1-THF synthase. In mitochondria, CHO-THF is a co-substrate

to generate formate by mitochondrial CHO-THF synthetase (M-4). Reaction M-4 is catalyzed by methylenetetrahydrofolate dehydrogenase (MTHFD1L, encoded by *MTHFD1L* gene, monofunctional C1-THF synthase in the mitochondria (Tibbetts & Appling 2010).

2 Materials and Methods

2.1 Generation of *Slc25a32* Mice

A transgenic mouse model of the gene *Slc25a32* was generated by microinjection of OmniBank ES cell clones (IST11480G10; encoding the gene *Slc25a32*) obtained from the Texas A&M Institute for Genomic Medicine. The gene trap mutations were produced by using the insertion of the gene trap vector, β-geo (*LacZ*) reporter (encoded by β-galactosidase) into ES cells derived from the C57BL/6 strain.

All experimental mice were housed in accordance with guidelines approved by the Institutional Animal Care and Use Committee (IACUC) of the University of Texas at Austin. Heterozygous *Slc25a32*$^{+/gt}$ breeding pairs were mated together in order to generate embryos of all genotypes. The morning following the introduction of heterozygous *Slc25a32*$^{+/gt}$ males, the *Slc25a32*$^{+/gt}$ dams aged 8-12 weeks were examined for the presence of a vaginal plug, which was indicative of gestational day 0.5 (E0.5). All mice were maintained on a PicoLab diet #20 (3 ppm of folic acid) and water, *ad libitum*, and were maintained on a 12-h light/dark cycle in a temperature-controlled room.

2.2 Embryo Collection and Morphological Evaluation

Pregnant dams were sacrificed by CO_2 asphyxiation and the embryos were removed from their decidual capsules and grossly examined under a dissecting microscope (Leica) for the presence of NTDs and other morphologic abnormalities. The number of somites were determined for each embryo as a hallmark of the development stage of the embryo. The crown-rump length (CRL) was quantitatively measured with the aid of dissecting microscope. Yolk sacs were collected for DNA extraction and genotyping, after which the

embryos were fixed in 10% neutral buffered formalin or stored at -80°C for biochemical analyses.

2.3 Genotyping Assays

Genomic DNA was extracted from the yolk sacs of embryos or the tail of young pups for genotyping assays. The samples were prepared by DirectPCR Lysis Reagent and Proteinase K (Viagen Biotech). The PCR genotyping was performed using one primer pair (5'-GGTGAAGGAAGGAGGAGCTT-3' and 5'-TCCACTGTTCAACATTAAGACACA -3') to detect the wild-type allele (266 bp) and the other primer pair (5'-GGTGAAGGAA GGAGG3AGCTT-3' and 5'-CCAATAAACCCTCTTGCAGTTGC-3') to detect the mutant allele (212 bp).

2.4 β-galactosidase (*LacZ*) Staining and Histology Analysis

For detecting reporter gene expression, the β-galactosidase staining of embryos at E9.5 was carried out using 5-bromo-4-chloro-3-indolyl-b-galactopyranoside (X-gal) stock (Sigma), marking a nuclear localized *lacZ* transgene. For histological analyses, the E11.5 fetuses were fixed in 10% neutral buffered formalin and embedded in paraffin. They were sectioned at 4-μm thickness and stained with hematoxylin/eosin (HE).

2.5 Reverse Transcriptase Polymerase Chain Reaction (RT-PCR) and Quantitative Real Time Polymerase Chain Reaction (qRT-PCR)

For RT-PCR analysis, total mRNA was extracted from whole mouse embryos of all *Slc25a32* potential genotypes at E10 using TRIzol Reagent (Invitrogen). First-strand cDNA was synthesized by cDNA Reverse Transcription Kit (Applied Biosystems). PCR was carried out with designed primer pairs of the *Slc25a32* gene forward (5'-

GGAGCCATGACTCTGTGCAT-3') and reverse (5'-TCCACCGATGCCTTCTTTCC-3') to amplify a 441 bp amplicon, and used β-actin primer as a positive control forward (5'-CCACCATGTACCCAGGCATT-3') and reverse (5'-AGGGTGTAAAACGCAGC TCA-3') (253 bp). For qRT-PCR analysis, the total mRNA was prepared from whole E9.5 embryos of all genotypes and cDNA was synthesized as described above. The mRNA levels were quantitatively measured by using SsoAdvanced Universal SYBR Green Supermix (Bio-Rad). The *Slc25a32* primers and β-actin primers were used as a control, as described above.

2.6 Immunoblot Analysis

To detect the SLC25A32 protein, mitochondria were isolated from whole E11.5 fetuses of all three genotypes using the Mitochondria Isolation Kit (Thermo Fisher Scientific). The samples were sonicated in RIPA lysis buffer (50mM Tris-HCl pH 8.0, 150mM NaCl, 0.1% Triton X-100, 0.5% sodium deoxycholate, 0.1% SDS, 0.1mM sodium orthovanadate, 1mM NaF, and Protease inhibitors tablet (Roche)). A Bradford assay was performed to determine the protein concentrations (Bio-Rad). The protein was immunoblotted with rabbit polyclonal anti-SLC25A32 (Thermo Fisher Scientific) at a concentration of 1:1000, GAPDH (Cell Signaling) as a control at a dilution of 1:5000, and 1RDye® 800CW Goat anti-Rabbit IgG (LI-COR) at a concentration of 1:10000 to probe the antibodies against the target protein.

2.7 RNA-Sequence Analysis

Total mRNA was isolated from three E9.0 whole *Slc25a32*$^{+/+}$ and *Slc25a32*$^{gt/gt}$ embryos using TRIzol Reagent (Invitrogen), as described above. The concentration of the

RNA was determined using a Nanodrop ND-1000 Spectrophotometer (NanoDrop Technologies). The integrity of RNA was evaluated using a 1% denaturing RNA gel and an Agilent Technologies 2100 Bioanalyzer. Sequencing of the cDNA libraries was carried out using the Illumina Hiseq 4000 (Quick Biology). Differentially expressed genes (DEGs) were determined by fold change > 1.5 (logFC > 0.58) and a $p < 0.05$, genes with < 1 count per million (cpm). All obtained datasets were analyzed for Gene Ontology (GO), Kyto Encyclopedia of Genes and Genomes (KEGG), and reactome analysis with enriched terms, and for Ingenuity Pathway Analysis (IPA) including the canonical pathway.

2.8 Folic Acid and Calcium Formate Supplementation

Slc25a32$^{+/gt}$ dams were randomly assigned to a control, a folic acid (5-mTHF), and a calcium formate supplementation group. The supplementation was administered daily, immediately after detection of the vaginal plug (0.5-dpc). In the folic acid group, pregnant dams were given 5-mTHF dissolved in distilled water by gavage (25 mg/kg or 50 mg/kg body weight). In the calcium formate group, pregnant dams were given 0.1M (2,500 mg) calcium formate·kg^{-1}· d^{-1} by directly in the drinking water based on an average water intake of 5 ml/d for a 25 g mouse and were continued throughout pregnancy.

2.9 Statistical Analysis

Genotyping frequencies were compared by Hardy-Weinberg equilibrium and analyzed using a χ^2 test. The data were analyzed by mean ± SE with Stud6ent's *t*-test and the any p values < 0.05 were considered statistically significant.

3 Results

3.1 Inactivation of *Slc25a32* Leads to Embryonic Lethality

Gene trap insertion of the β-geo reporter locus between exons 1 and 2, resulted in a loss-of-function mutation (Fig. 2a). The genotype of *Slc25a32* (Fig. 2b) was determined by PCR using primers as shown in Fig. 2a. Reverse transcription PCR (RT-PCR) was performed to confirm the absence of *Slc25a32* mRNA in the $Slc25a32^{gt/gt}$ embryos (Fig. 3a). The SLC25A32 protein was not detected in isolated mitochondria of the $Slc25a32^{gt/gt}$ embryos by immunoblot analysis (Fig. 3b). These data indicate that the homozygous gene trap insertion of the *Slc25a32* successfully disrupted at both the RNA and protein levels.

To detect the reporter β-galactosidase (*LacZ*) gene and determine its expression and transfection efficiency, we stained embryos at the beginning of NTC. The activity of β-galactosidase detected in the $Slc25a32^{gt/gt}$ was compared to the $Slc25a32^{+/+}$ at E9.5, demonstrating that the *Slc25a32* message is ubiquitously expressed in the neural tube along the entire length of the developing embryo (Fig. 4a). Quantitative real-time PCR (qRT-PCR) was performed on RNA isolated from the $Slc25a32^{gt/gt}$ and the $Slc25a32^{+/+}$ E9.5 embryos to determine the extent of the knockout of the *Slc25a32* mRNA caused by inserting the gene-trap cassette. The mRNA levels of the $Slc25a32^{gt/gt}$ revealed very little expression compared to the $Slc25a32^{+/+}$, suggesting that the reduced expression of the *Slc25a32* mRNA contributes to the observed NTDs in the nullizygous embryos (Fig. 4b).

a.

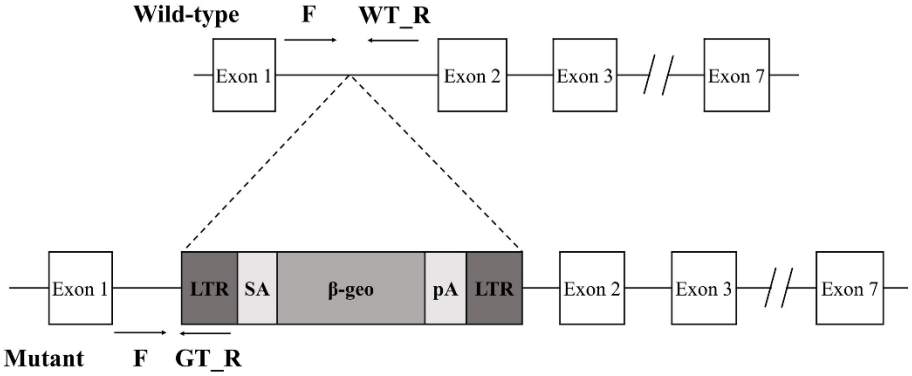

b.

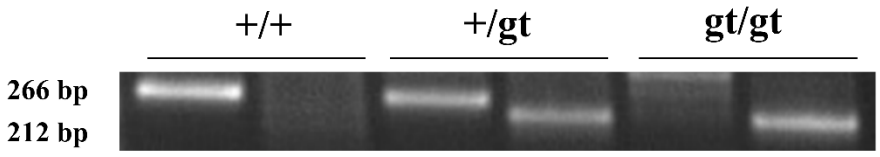

Figure 2. Genomic Structure of *Slc25a32* gene and Genotype

Fig. 2a. Genomic Structure of *Slc25a32* Gene and Gene Trapping Vector Design. This schema illustrates the genomic structure of the *Slc25a32* gene. Gene trap insertion of a β-geo cassette in the *Slc25a32* locus between exons 1 and 2. The *Slc25a32* gene is disrupted by inserting the β-geo (*LacZ*) that encodes β-galactosidase. The arrows indicate location of genotyping forward (F) and reverse (R) primers, wild-type (+/+) and mutant (gt/gt) alleles, respectively. LTR: viral long terminal repeat, SA: splice acceptor, pA: polyA. Fig. 2b. Genotyping Assays. The extracted genomic DNA is used for PCR genotyping. The banding pattern of the PCR products demonstrate the wild-type allele (266 bp) and the mutant allele (212 bp).

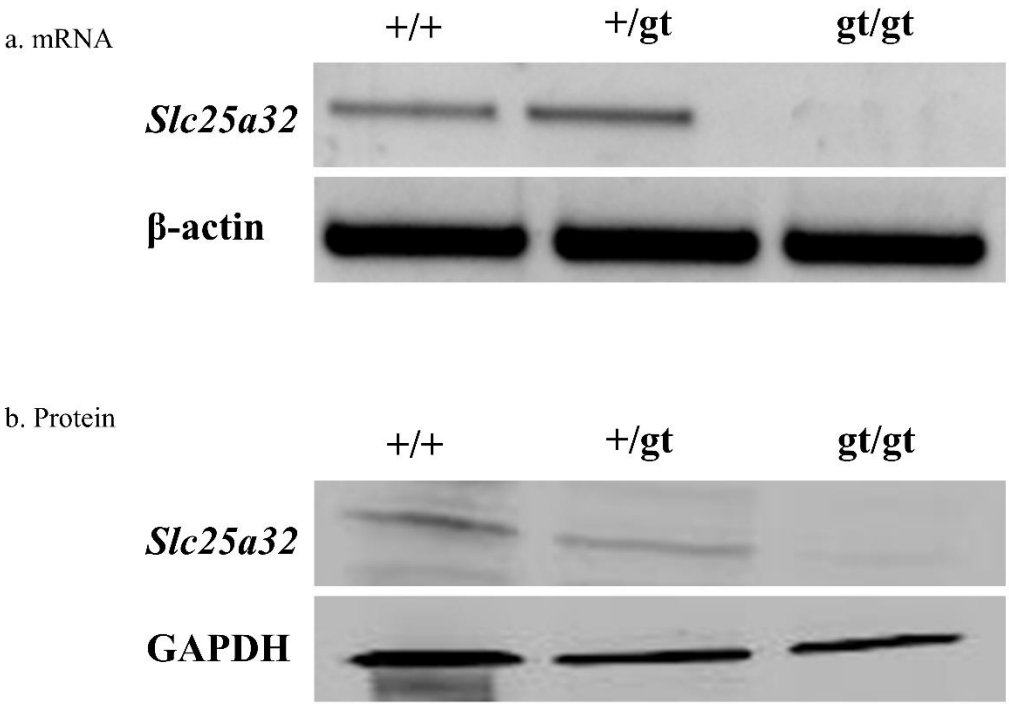

Figure 3. Reverse-Transcriptase (RT)-PCR for mRNA and Immunoblot Assay for Protein

Fig. 3a. RT-PCR for mRNA. *Slc25a32* mRNA expression was determined in E10 embryos of each possible genotype. Reverse transcription polymerase chain reaction (RT-PCR) analysis was performed with *Slc25a32*, using β-actin primer as a positive control for cDNA synthesis. Fig. 3b. Immunoblot Assay for Protein. SLC25A32 protein was detected from isolated mitochondria from E11.5 embryos of each potential genotype. The immunoblot assay was performed with anti-SLC25A32 antibody and anti-GAPDH (glyceraldehyde-3-phosphate dehydrogenase) antibody as a loading control.

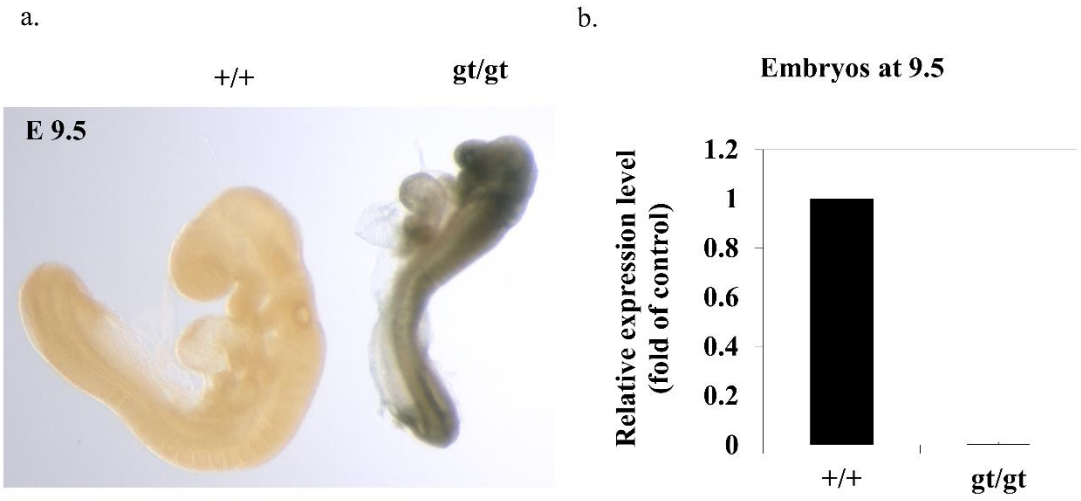

Figure 4. *Slc25a32* Gene Expression of β-galactosidase (*LacZ*) Staining and Quantitative Real-Time (qRT)-PCR at E9.5

Fig. 4a. β-galactosidase (*LacZ*) Staining at E9.5. Whole mount *LacZ* staining of nullizygous and wild-type embryos at E9.5. β-galactosidase was ubiquitously expressed in the *Slc25a32*$^{gt/gt}$ relative to the *Slc25a32*$^{+/+}$ embryos. Fig. 4b. Quantitative Real-time PCR (cDNA) at E9.5. The quantitative real-time PCR (qRT-PCR) illustrates mRNA levels of *Slc25a32* gene expression. The mRNA was reverse transcribed into cDNA from all E9.5 embryos of all possible genotypes. The qRT-PCR analysis was performed with *Slc25a32* primer and β-actin primer was used as a house-keeping gene.

Heterozygous *Slc25a32*$^{+/gt}$ mice were intercrossed with the intention of generating the wild-type (*Slc25a32*$^{+/+}$), homozygous mutant (*Slc25a32*$^{gt/gt}$) and heterozygous (*Slc25a32*$^{+/gt}$) mice. We collected a total of 63 litters and 357 live-born young, with an average litter size of 5.5 pups per each *Slc25a32*$^{+/gt}$ dam. Initial breeding of the *Slc25a32*$^{+/gt}$ mice failed to produce any viable live-born *Slc25a32*$^{gt/gt}$ pups, suggesting that homozygous loss of functional *Slc25a32* alleles is a lethal mutation. To determine when the *Slc25a32*$^{gt/gt}$ embryos die *in utero*, the *Slc25a32*$^{+/gt}$ mice were intercrossed in timed matings, and the dams were euthanized between E9.5-12.5 and uterine contents were analyzed. There were no *Slc25a32*$^{gt/gt}$ fetuses beyond E12.5. In total, 271 fetuses were examined between E10-12.5, in addition to 31 resorptions from 35 litters. The yolk sac of all conceptions were used for PCR genotyping. Genotyping indicated there were 76 *Slc25a32*$^{+/+}$, 135 *Slc25a32*$^{+/gt}$, and 60 *Slc25a32*$^{gt/gt}$ fetuses (Table 1). Specifically, 143 embryos between E10-10.5 were collected along with 18 resorptions from 18 pregnant dams. There were 43 *Slc25a32*$^{+/+}$, 73 *Slc25a32*$^{+/gt}$, and 27 *Slc25a32*$^{gt/gt}$ embryos. Of 92 embryos collected between E11-11.5 were obtained with six resorptions from 12 pregnant dams. There were 25 *Slc25a32*$^{+/+}$, 47 *Slc25a32*$^{+/gt}$, and 20 *Slc25a32*$^{gt/gt}$ embryos. From 5 pregnant dams, 36 embryos were examined with 7 resorptions and displayed 10 *Slc25a32*$^{+/+}$, 14 *Slc25a32*$^{+/gt}$, and 12 *Slc25a32*$^{gt/gt}$ embryos between E12-12.5. The genotyping results were consistent with a Hardy-Weinberg Equilibrium (*p*-HWE) ($p = 1.00$) (Table 1-2). We performed sex-receptor Y (SRY) genotyping to examine whether disruption of the *Slc25a32* gene contributed to an increased prevalence of NTD affected male or female embryos. There did not appear to be any gender bias in NTD susceptibility (data not shown). The loss of

Slc25a32 function results in embryo lethality, demonstrating that the *Slc25a32* gene is essential during mouse embryonic development.

	No. of litters	No. of implants	No. of resorptions	No. of *Slc25a32*$^{+/+}$	No. of *Slc25a32*$^{+/gt}$	No. of *Slc25a32*$^{gt/gt}$	No. of NTDs in *Slc25a32*$^{gt/gt}$	% of NTDs in *Slc25a32*$^{gt/gt}$	*p*-HWE
E10-10.5	18	161	18	41	74	28	28	100	
E11-11.5	12	98	6	25	47	20	20	100	1.00
E12-12.5	5	42	7	10	14	12	12	100	

Table 1. The Number of NTDs in Unsupplemented *Slc25a32*$^{gt/gt}$ Embryos at E10-12.5

p-value of Hardy-Weinberg Equilibrium (*p*-HWE)

Genotypes	Observed #	Expected #
Slc25a32$^{+/+}$	76	76.0
Slc25a32$^{+/gt}$	135	135.0
Slc25a32$^{gt/gt}$	60	60.0
Var allele freq	0.47	
χ^2	1.13843E-05	
X^2 test *P* value	0.997308	

Table 2. The *p* value of Hardy-Weinberg Equilibrium (p-HWE) on Genotype Distribution of Unsupplemented *Slc25a32* Embryos at E10-12.5

p-value of Hardy-Weinberg Equilibrium (*p*-HWE)

3.2 Depletion of *Slc25a32* Causes a Failure of Neural Tube Closure

As described above, disruption of the *Slc25a32* gene adversely affects early embryonic development. All *Slc25a32*$^{gt/gt}$ fetuses lose viability by E12.5. From the *Slc25a32*$^{+/gt}$ dams, embryos and fetuses from all three potential genotypes were examined on different embryonic days to determine the prevalence of NTC defects. All *Slc25a32*$^{gt/gt}$ embryos present with abnormal phenotypes during the period of NTC. They exhibited 100% penetrant NTDs that were confined primarily to the rostral cranial region, although on occasion extending into the cervical or thoracic regions. None of the *Slc25a32*$^{+/+}$ and *Slc25a32*$^{+/gt}$ embryos showed NTDs. The majority of NTDs observed in the *Slc25a32*$^{gt/gt}$ embryos at E10.5 were exencephaly, indicating that the fusion of neural tube from the forebrain to the midbrain failed to close completely (Fig. 5a). The *Slc25a32*$^{gt/gt}$ E10.5 embryos presented with an open neural tube from the forebrain to the hindbrain, as well as craniofacial defects (Fig. 5b-c). As shown in Fig. 5d, the *Slc25a32*$^{gt/gt}$ embryos displayed craniorachischisis at E12.5, with an open neural tube extending from the cervical boundary to the forebrain. The *Slc25a32*$^{gt/gt}$ fetuses primarily exhibited exencephaly at E12.5 (Fig. 5e-f). All *Slc25a32*$^{gt/gt}$ embryos had open rostral NTDs in the cranial region at E10.5 or E12.5. Among 60 *Slc25a32*$^{gt/gt}$ fetuses evaluated morphologically between E10-12.5, 18 fetuses had NTC defects from the forebrain to the midbrain, 7 embryos displayed open midbrain NTDs, 26 fetuses examined had an open, unfused neural tube extending from the midbrain to the hindbrain, and 9 fetuses presented with craniorachischisis. As shown in Fig. 6, hematoxylin/eosin (HE) stained histological sections revealed that E11.5 *Slc25a32*$^{gt/gt}$ embryos exhibited unfused neural folds at the level of the forebrain and the

midbrain (Fig. 6d-e), which was never observed in *Slc25a32*$^{+/+}$ embryos (Fig. 6b-c). Clearly, a functional deficiency of the *Slc25a32* gene resulted in the observed dysmorphology and 100% penetrance for NTDs in the mutant mouse.

Additionally, we observed differences in the developmental growth of the fetuses of different *Slc25a32* genotypes, most noticeably in the crown-rump measurements after NTC at E11.5. As shown in Fig. 7a-b, the *Slc25a32*$^{gt/gt}$ (2.97 ± 0.26) fetuses were significantly smaller than the *Slc25a32*$^{+/+}$ (3.97 ± 0.16) at E11.5, suggesting that the functional absence of the *Slc25a32* gene results in a significant inhibition of embryonic growth ($p < 0.05$).

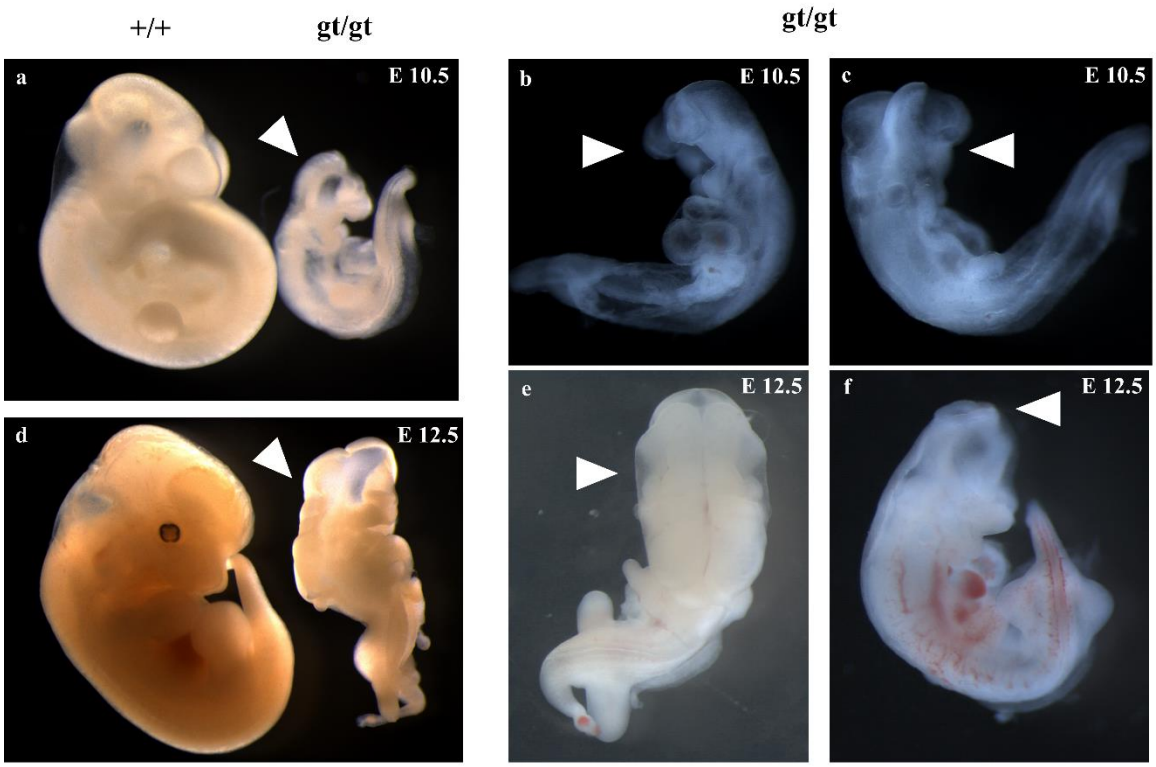

Figure 5. Embryonic NTDs in Unsupplemented *Slc25a32*$^{gt/gt}$ Embryos at E10.5 and E12.5

Fig. 5a. The *Slc25a32*$^{gt/gt}$ embryos display open neural tubes from the forebrain to the midbrain at E10.5. Arrows indicate unfused neural folds at cranial portion of the *Slc25a32*$^{gt/gt}$ embryos. Fig. 5b and 5c. Arrow indicate that the nullizygous (*Slc25a32*$^{gt/gt}$) embryos had exencephaly and facial defects at E10.5. Fig. 5d. At E12.5, the *Slc25a32*$^{gt/gt}$ embryos presents with an open neural tube from the forebrain to the hindbrain. Fig. 5e and 5f. Arrow indicate that the nullizygous (*Slc25a32*$^{gt/gt}$) embryos exhibited craniorachischisis (5e) and exencephaly (5f) at E12.5.

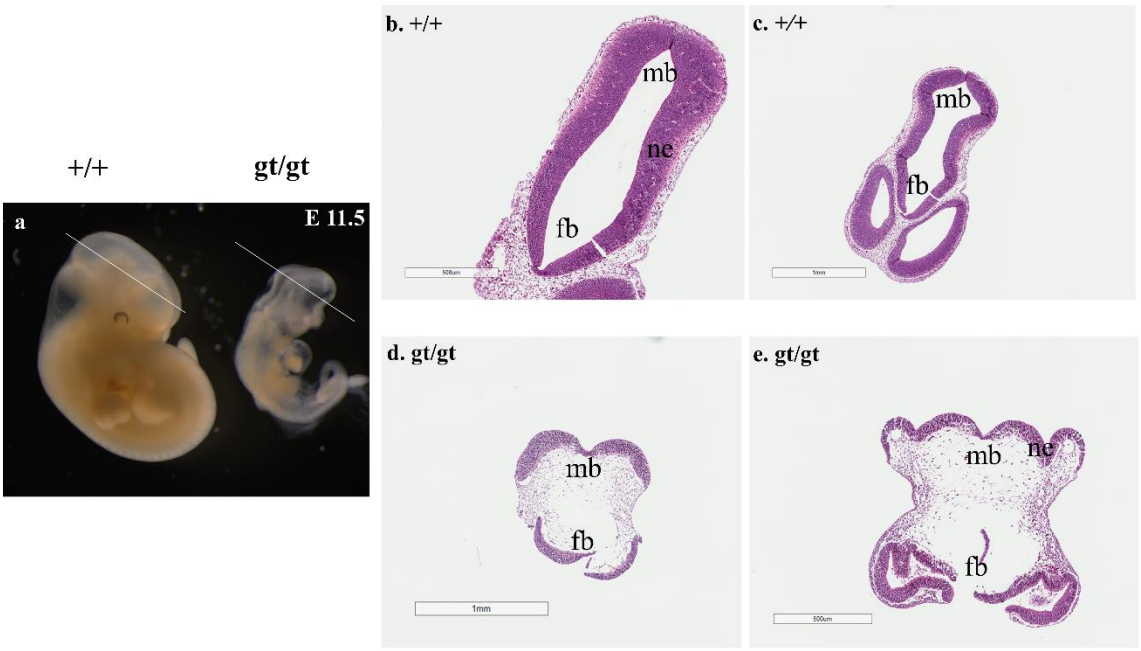

Figure 6. Embryonic Histological Analysis of *Slc25a32* Embryos at E11.5

Fig. 6a. The location of the histological sections of the *Slc25a32* embryos at E11.5 is at the level of the forebrain and the midbrain. In Fig. 6b and 6c, arrows indicate the $Slc25a32^{+/+}$ embryo with fused neural folds at the level of the forebrain and the midbrain. In Fig. 6d and 6e, arrows indicate the $Slc25a32^{gt/gt}$ embryo with unfused neural folds, precursors for an exencephaly and facial defects. Scale bars are 1 mm (c and d) and 500 μm (b and e). fb, forebrain; mb, midbrain; ne, neuroepithelium

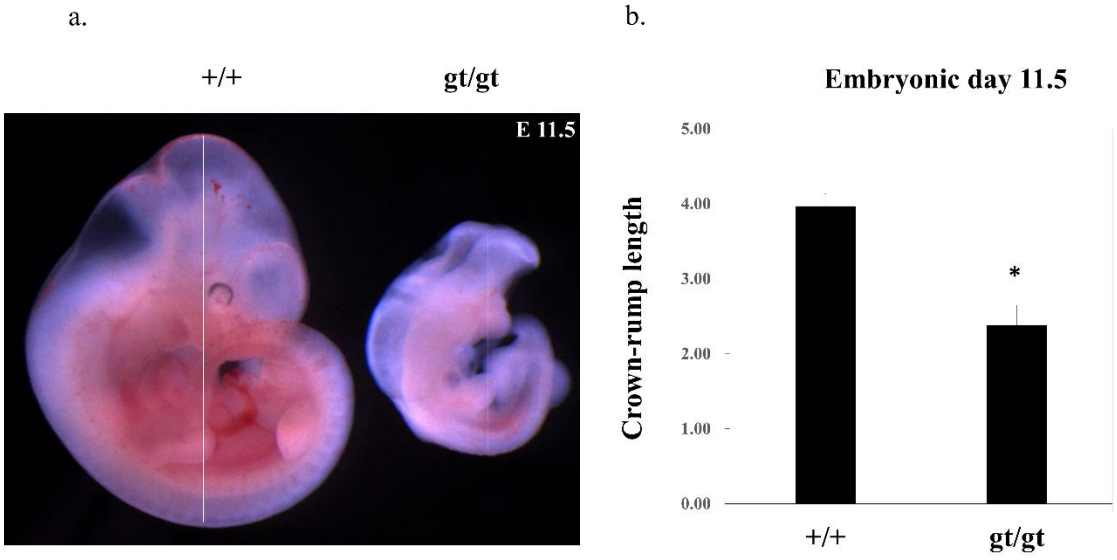

Figure 7. Embryonic Crown-rump Length in Unsupplemented *Slc25a32* Embryos at E11.5

Fig. 7a. The *Slc25a32*$^{gt/gt}$ embryos represented an open neural tube and growth retardation compared to the *Slc25a32*$^{+/+}$ embryos at E11.5. Fig. 7b. The bar chart indicates the embryonic crown-rump length differences between the *Slc25a32*$^{+/+}$ and the *Slc25a32*$^{gt/gt}$ embryos at E11.5. (*$p < 0.05$).

3.3 Effect of Maternal Folic Acid and Calcium Formate Supplementation in *Slc25a32* Deficient Mouse

Mitochondrial folate-mediated 1C pathway produces formate to support purine biosynthesis. Disruption of the *Slc25a32* gene affects the transport of THF into the mitochondria and interrupts the generation of formate, which is a downstream output product of the mitochondrial folate pathway. The *Slc25a32*$^{+/gt}$ dams were supplemented with either 5-mTHF or calcium formate from the time the pregnancy was recognized (E0.5) throughout gestation. The *Slc25a32*$^{+/gt}$ dams were supplemented with 5-mTHF (25 mg/kg or 50 mg/kg body weight) by oral gavage and with 0.1M (a calculated dose of 2,500 mg/kg/day) calcium formate in their drinking, respectively. The maternal supplementation of 5-mTHF in the *Slc25a32*$^{+/gt}$ dams lose viable *Slc25a32*$^{gt/gt}$ fetuses by E12.5. With both 25 mg/kg and 50 mg/kg of 5-mTHF supplementation, we observed 53 fetuses and 4 resorptions from 6 litters between E10-12.5. Genotyping revealed that there were 12 *Slc25a32*$^{+/+}$, 26 *Slc25a32*$^{+/gt}$, and 11 *Slc25a32*$^{gt/gt}$ fetuses (Table 3). The genotyping results were consistent with a Hardy-Weinberg Equilibrium (p-HWE) (p = 0.67) (Table 3-4). All of 11 *Slc25a32*$^{gt/gt}$ fetuses had open NTDs, suggesting that maternal FA (5-mTHF) supplementation is not responsive to rescue the NTDs, similar to the unsupplemented *Slc25a32*$^{+/gt}$ mice. The maternal supplementation of calcium formate in the *Slc25a32*$^{+/gt}$ intercrossed mice also failed to generate any viable *Slc25a32*$^{gt/gt}$ pups, which mirrored our experience with the unsupplemented *Slc25a32*$^{+/gt}$ mouse. By harvesting litters at selected timepoints during embryogenesis, we determined that the *Slc25a32*$^{gt/gt}$ fetuses receiving the calcium formate supplementation remain viable until E15.5. In total, we examined 185

fetuses between E10-15.5, in addition to 14 resorptions obtained from 23 litters. Genotyping revealed that there were 44 *Slc25a32*$^{+/+}$, 95 *Slc25a32*$^{+/gt}$, and 32 *Slc25a32*$^{gt/gt}$ fetuses (Table 5). The population is in Hardy-Weinberg Equilibrium (*p*-HWE) ($p = 0.13$) (Table 5-6). With *in utero* calcium formate supplementation, 25 *Slc25a32*$^{gt/gt}$ fetuses had a normal phenotype and a completely closed neural tube (Fig. 8), while 7 *Slc25a32*$^{gt/gt}$ fetuses had open NTDs (Table 5). This data suggests that 0.1M calcium formate partially rescues the NTDs by facilitating the closing of the neural tube in a majority of the *Slc25a32*$^{gt/gt}$ fetuses.

5-Methyl-THF (5-mTHF)	No. of litters	No. of implants	No. of resorptions	No. of *Slc25a32*$^{+/+}$	No. of *Slc25a32*$^{+/gt}$	No. of *Slc25a32*$^{gt/gt}$	No. of NTDs in *Slc25a32*$^{gt/gt}$	% of NTDs in *Slc25a32*$^{gt/gt}$	*p*-HWE
25 mg/kg	3	30	4	6	14	6	6	100	0.67
50 mg/kg	3	23	0	6	12	5	5	100	

Table 3. The Impact of Maternal Folic Acid (5-mTHF) Supplementation on NTC in *Slc25a32*$^{gt/gt}$ Embryos at E10-12.5

p-value of Hardy-Weinberg Equilibrium (*p*-HWE)

Genotypes	Observed #	Expected #
Slc25a32$^{+/+}$	12	12.8
Slc25a32$^{+/gt}$	26	24.5
Slc25a32$^{gt/gt}$	11	11.8
Var allele freq	0.49	
χ^2	0.186336111	
X^2 test *P* value	0.665984	

Table 4. The *p* value of Hardy-Weinberg Equilibrium (p-HWE) on Genotype Distribution of Maternal Folic Acid (5-mTHF) Supplemented in *Slc25a32* embryos at E10-12.5

p-value of Hardy-Weinberg Equilibrium (*p*-HWE)

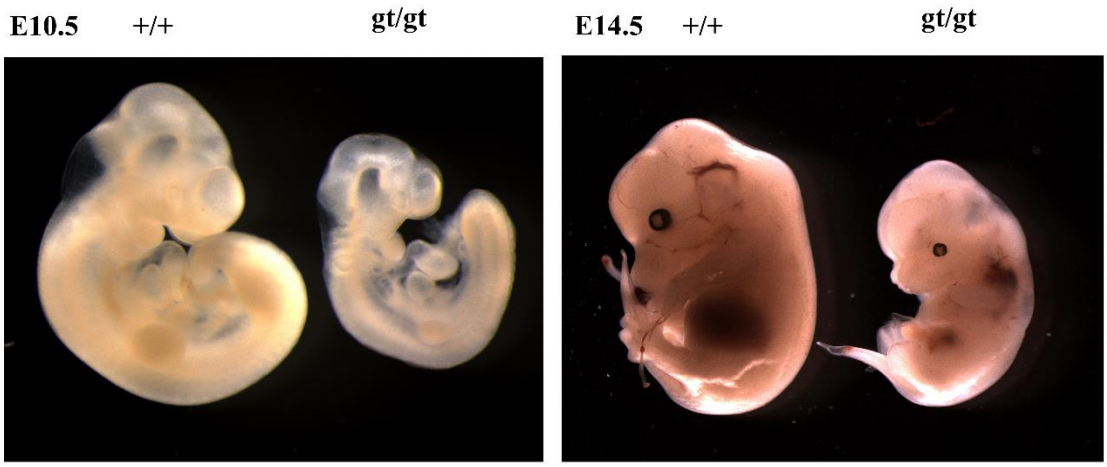

Figure 8. Effects of Maternal Calcium Formate Supplementation in *Slc25a32*$^{gt/gt}$ Embryos at E10.5 and E14.5

The impact of periconceptional calcium formate supplementation on neural tube closure in the *Slc25a32*$^{gt/gt}$ embryos at E10.5 and E14.5.

	No. of litters	No. of implants	No. of resorptions	No. of *Slc25a32*$^{+/+}$	No. of *Slc25a32*$^{+/gt}$	No. of *Slc25a32*$^{gt/gt}$	No. of NTDs in *Slc25a32*$^{gt/gt}$	No. of NTC in *Slc25a32*$^{gt/gt}$	*p*-HWE
E10-10.5	8	64	3	15	29	17	2	15	
E13-13.5	7	59	4	18	29	8	4	4	0.13
E15-15.5	8	62	7	11	37	7	1	6	

Table 5. The Impact of Maternal Calcium Formate Supplementation on NTC in *Slc25a32*$^{gt/gt}$ Embryos at E10-15.5

p-value of Hardy-Weinberg Equilibrium (*p*-HWE)

Genotypes	Observed #	Expected #
Slc25a32$^{+/+}$	44	49.0
Slc25a32$^{+/gt}$	95	85.1
Slc25a32$^{gt/gt}$	32	37.0
Var allele freq	0.46	
χ^2	2.325237945	
X^2 test *P* value	0.127291	

Table 6. The *p* value of Hardy-Weinberg Equilibrium (p-HWE) on Genotype Distribution of Maternal Calcium Formate Supplemented in *Slc25a32* embryos at E10-15.5

p-value of Hardy-Weinberg Equilibrium (*p*-HWE)

3.4 RNA-Seq Profiling of *Slc25a32* Knockout Embryos at E9.0

To identify gene dysregulation across the transcriptome following the inactivation of *Slc25a32*, we carried out RNA-seq analysis with three wild-type ($Slc25a32^{+/+}$) and three nullizygous ($Slc25a32^{gt/gt}$) E9.0 embryos (Fig. 9a). Differential expression analysis identified 1,092 genes that were upregulated, while 630 genes were downregulated (Fig. 10). Of these, the expression level of the *Slc25a32* significantly decreased in the $Slc25a32^{gt/gt}$ embryos compared with the $Slc25a32^{+/+}$ embryos (Fig. 9b). Gene ontology (GO) analysis revealed enrichment for genes ($p < 0.05$) involved in blood circulation, muscle tissue development, cellular ion homeostasis, regulation of cell morphogenesis, and cell fate commitment. The cellular component of GO categories was enriched including lytic vacuole, lysosome, cell-cell junction, apical part of cell, and extracellular matrix. Among the GO enrichment in molecular function categories, the list included: transcriptional activator activity, RNA polymerase II transcription regulatory region sequence-specific binding, core promoter proximal region DNA binding, actin binding, protein heterodimerization activity, and active transmembrane transporter activity (Fig. 11). As shown in Table 7, the list revealed multiple dysregulated 1C metabolic process genes, as might be expected. The upregulated genes include *Fpgs* (Folylpolyglutamyl synthetase) and *Mthfs* (5, 10- Methenyltetrahydrofolate synthetase) while downregulated genes of interest include *Dhfr* (Dihydrofolate reductase) and *Mthfd2l* (Methylene-tetrahydrofolate dehydrogenase (NADP-dependent) 2-like), both are important enzymes involved in folate-mediated 1C metabolism. Among the genes whose transcription was significantly altered, there are several genes that have previously been reported to be

associated with an increased risk for NTDs, providing validation of our results. Among the upregulated genes, these included: *cdx2* (caudal type homeobox 2) and *Fbln1* (fibulin1), both of which are highly expressed and they may be relevant to mediating events during NTC (Table 8) (Savory et al. 2011) (Cooley et al. 2008). Several of the most significantly downregulated genes include: *Lhx9* (LIM homeobox protein 9) and *Neurod1* (neurogenic differentiation 1) related to neuronal differentiation (Peukert et al. 2011) (Boutin et al. 2010), *Epha3* (Eph receptor A3) associated with epithelial fusion during neural tube morphogenesis (Abdul-Aziz et al. 2009) and *Pax3* and *Zic2* transcription factors (Table 9) (Epstein, Vekemans, and Gros 1991) (Carrel et al. 2000) (Ybot-Gonzalez et al. 2007). All of these represent interesting candidate genes for future interrogation. Considering the ingenuity canonical (IPA) pathway, there are several upregulated or downregulated pathways related to the regulation of genes involved in NTC, including upregulation of PCP pathway (Wu et al. 2011) and downregulation of Rho family GTPase (Kinoshita et al. 2008) and RhoA signaling (Nishimura, Honda, and Takeichi 2012) (Fig. 12-13).

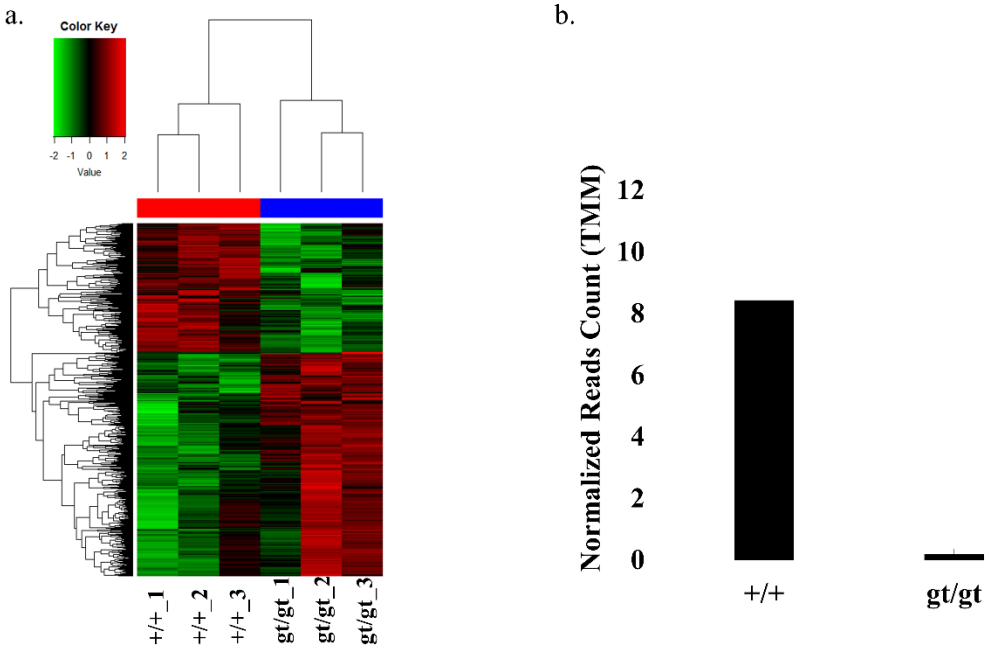

Figure 9. RNA-Seq Analysis of Inactivation *Slc25a32* Gene in Embryos at E9.0

Fig. 9a. Heat map of RNA-Seq data indicates the differentially expressed genes (DEGs) pattern between *Slc25a32*$^{+/+}$ (n=3) and *Slc25a32*$^{gt/gt}$ (n=3) E9.0 embryos. Fig. 9b. RNA-Seq data shows the expression level of *Slc25a32* by normalized reads counts (TMM) in the *Slc25a32*$^{gt/gt}$ embryos compared to the *Slc25a32*$^{+/+}$ embryos at E9.0

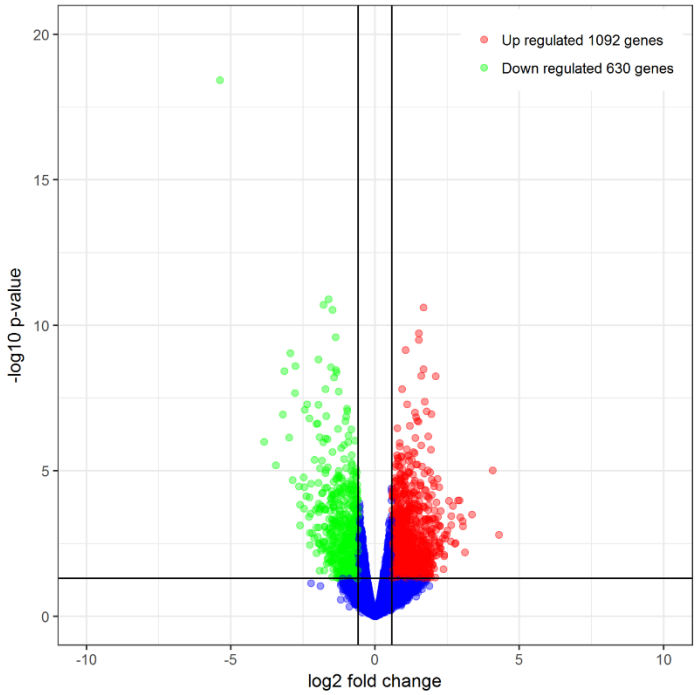

Figure 10. Volcano Plot of RNA-Seq Analysis

RNA-Seq data identified the upregulated 1,092 genes and the downregulated 630 genes in the *Slc25a32*$^{gt/gt}$ embryos compared to the *Slc25a32*$^{+/+}$ embryos at E9.0.

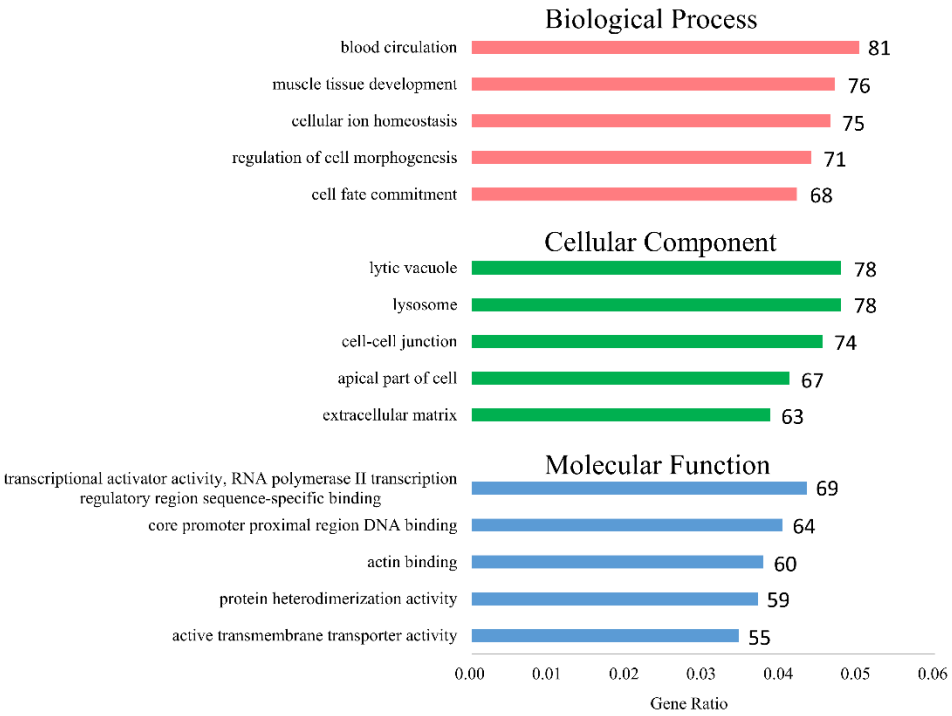

Figure 11. Gene Ontology (GO) Enrichment of RNA-Seq Analysis

RNA-Seq data reveals Gene Ontology (GO) enrichment with the top five classifications including; biological process, cellular component, and molecular function in the *Slc25a32*$^{gt/gt}$ embryos compared to the *Slc25a32*$^{+/+}$ embryos at E9.0. In bars, the numbers represent the numbers of dysregulated genes in each ontological classification ($p < 0.05$).

Gene Symbol	Gene Name	FC	*P* Value	FDR
Car2	Carbonic anhydrase 2	-1.89	0.0009	0.0233
Car4	Carbonic anhydrase 4	2.91	0.0007	0.0182
Dhfr	Dihydrofolate reductase	-1.52	4.44E-05	0.0032
Dmgdh	Dimethylglycine dehydrogenase precursor	3.06	0.0044	0.0606
Fpgs	Folylpolyglutamyl synthetase	1.50	0.0069	0.0803
Mthfd2l	Methylenetetrahydrofolate dehydrogenase (NADP+ dependent) 2-like	-1.58	0.0039	0.0551
Mthfs	5, 10-methenyltetrahydrofolate synthetase	2.07	0.0283	0.1825

Table 7. List of Dysregulated One Carbon Metabolic Process Genes in *Slc25a32*$^{gt/gt}$ versus *Slc25a32*$^{+/+}$ at E9.0

FC, fold change; FDR, false discovery rate

Gene Symbol	Gene Name	FC	*P* Value	FDR
Fgfr4	Fibroblast growth factor receptor 4	4.50	1.87E-05	0.0019
Angptl6	Angiopoietin-like 6	3.37	4.72E-05	0.0034
Gdf1	Growth differentiation factor 1	3.29	4.47E-05	0.0032
Cdx4	Caudal type homeobox 4	2.68	1.45E-07	4.95E-05
Foxf1	Forkhead box F1	2.15	5.19E-08	2.39E-05
Lama5	Laminin, alpha 5	2.08	7.05E-10	8.75E-07
Cdx2	Caudal type homeobox 2	2.02	1.48E-05	0.0017
Ptch1	Patched homolog 1	1.87	3.39E-06	0.0006
Nid2	Nidogen 2	1.81	1.46E-06	0.0003
Nav2	Neuron navigator 2	1.73	3.74E-06	0.0006
Amot	Angiomotin	1.63	1.73E-05	0.0018
Flnc	Filamin C, gamma	1.60	5.52E-05	0.0037
Fbln1	Fibulin 1	1.54	7.45E-05	0.0043

Table 8. List of Dysregulated Upregulation Genes Associated with NTDs in *Slc25a32*$^{gt/gt}$ versus *Slc25a32*$^{+/+}$ at E9.0

FC, fold change; FDR, false discovery rate

Gene Symbol	Gene Name	FC	*P* Value	FDR
Slc25a32	Solute carrier family 25, member 32	-41.44	3.69E-19	1.68E-15
Nhlh2	Nescient helix loop helix 2	-8.88	3.69E-09	2.80E-06
Zic4	Zinc finger protein of the cerebellum 4	-7.91	7.08E-07	0.0002
Lhx9	LIM homeobox protein 9	-7.69	8.91E-10	1.01E-06
Neurod1	Neurogenic differentiation 1	-6.82	2.51E-09	2.45E-06
Neurod4	Neurogenic differentiation 4	-4.27	4.16E-06	0.0007
Wnt8b	Wingless-type MMTV integration site family, member 8B	-3.99	2.34E-07	7.09E-05
Dcx	Doublecortin	-3.76	8.14E-06	0.0011
Neurog1	Neurogenin 1	-3.59	4.40E-06	0.0007
Wnt9a	Wingless-type MMTV integration site family, member 9A	-3.58	5.96E-05	0.0038
Epha3	Eph receptor A3	-3.29	1.20E-05	0.0014
Emx2	Empty spiracles homeobox 2	-3.25	1.32E-07	4.67E-05
Olig3	Oligodendrocyte transcription factor 3	-3.14	8.19E-07	0.0002
Tubb3	Tubulin, beta 3 class III	-3.05	1.25E-11	4.27E-08
Pax3	Paired box 3	-2.89	2.72E-09	2.48E-06
Pax7	Paired box 7	-2.89	8.59E-05	0.0048
Meox2	Mesenchyme homeobox 2	-2.85	4.88E-05	0.0034
Dbx1	Developing brain homeobox 1	-2.81	6.81E-05	0.0041
Zic1	Zinc finger protein of the cerebellum 1	-2.78	2.89E-11	5.63E-08
Msx3	Msh homeobox 3	-2.57	6.04E-05	0.0038
Pax6	Paired box 6	-2.56	3.38E-09	2.72E-06
Wnt7b	Wingless-type MMTV integration site family, member 7B	-2.47	5.36E-05	0.0036
Meox1	Mesenchyme homeobox 1	-2.40	9.86E-06	0.0013
Zic3	Zinc finger protein of the cerebellum 3	-2.33	3.93E-05	0.0030
Lhx2	LIM homeobox protein 2	-2.27	1.66E-06	0.0003
Tfap2b	Transcription factor AP-2 beta	-2.12	1.28E-06	0.0003
Lrrn1	Leucine rich repeat protein 1, neuronal	-2.11	3.95E-06	0.0007
Crabp2	Cellular retinoic acid binding protein II	-1.97	7.35E-08	3.24E-05
Nes	Nestin	-1.92	1.04E-06	0.0002
Zic2	Zinc finger protein of the cerebellum 2	-1.85	6.01E-05	0.0038
Sox11	SRY (sex determining region Y)-box 11	-1.80	2.15E-05	0.0021
Gas1	Growth arrest specific 1	-1.78	9.79E-06	0.0013
Sfrp2	Secreted frizzled-related protein 2	-1.76	4.95E-05	0.0035
Sox2	SRY (sex determining region Y)-box 2	-1.76	6.82E-05	0.0041
Sema3a	Sema domain, immunoglobulin domain (Ig), short basic do main, secreted, (semaphorin) 3A	-1.67	2.95E-05	0.0025
Crabp1	Cellular retinoic acid binding protein I	-1.62	3.46E-05	0.0028
Gas5	Growth arrest specific 5	-1.57	1.62E-05	0.0018
Meis1	Meis homeobox 1	-1.55	6.29E-05	0.0039
Dhfr	Dihydrofolate reductase	-1.52	4.44E-05	0.0032

Table 9. List of Dysregulated Downregulation Genes Associated with NTDs in *Slc25a32*$^{gt/gt}$ versus *Slc25a32*$^{+/+}$ at E9.0

FC, fold change; FDR, false discovery rate

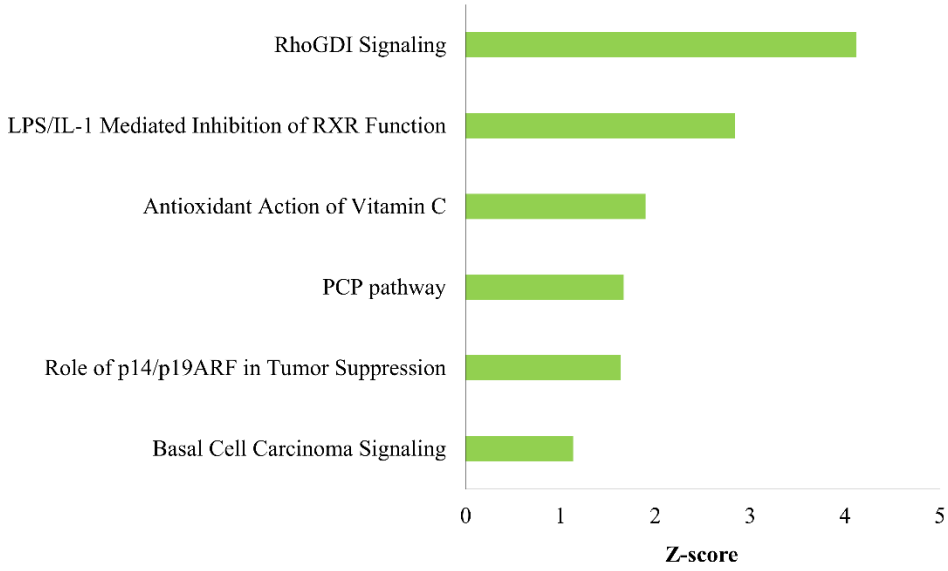

Figure 12. Downregulation of Ingenuity Canonical Pathway in RNA-Seq Analysis

Ingenuity Canonical Pathway indicates downregulation in the *Slc25a32*$^{gt/gt}$ embryos compared to the *Slc25a32*$^{+/+}$ embryos at E9.0.

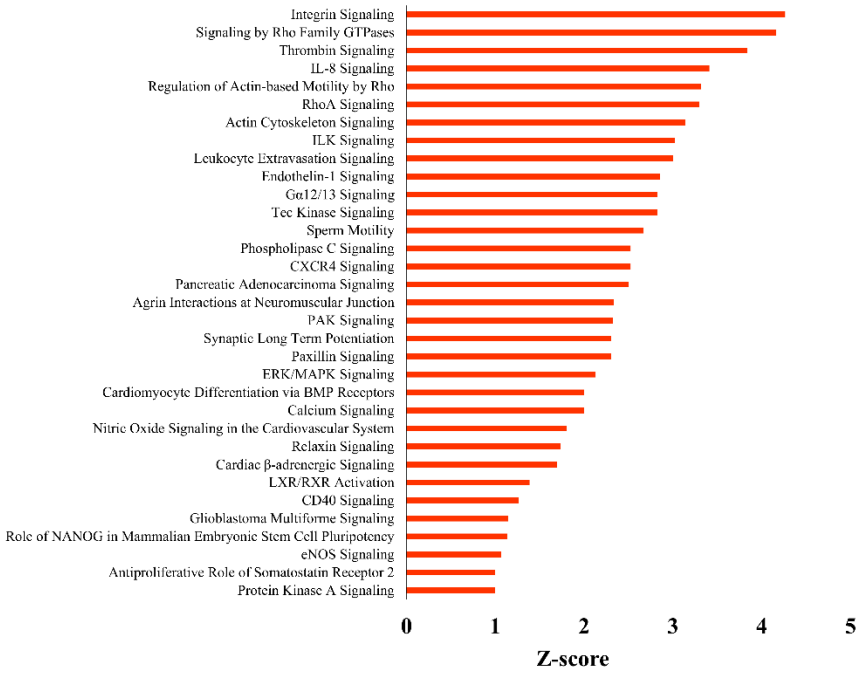

Figure 13. Upregulation of Ingenuity Canonical Pathway in RNA-Seq Analysis

Ingenuity Canonical Pathway indicates upregulation in the *Slc25a32*$^{gt/gt}$ embryos compared to the *Slc25a32*$^{+/+}$ embryos at E9.0.

4 Discussion

Low folate status has been known to increase the risk for an NTD affected pregnancy. Studies conducted over the past 30 years have consistently shown that periconceptional supplementation with FA can reduce the prevalence of NTDs. While maternal FA supplementation may prevent up to 70% of NTDs (MRC Vitamin Study Research Group 1991), non-folate responsive NTDs remain a significant health care concern. We observed that genetic disruption of *Slc25a32* in mice results in NTDs that are not responsive to maternal folate supplementation.

In humans, a *SLC25A32* polymorphism in a Japanese population of post-menopausal women was linked to plasma folate levels and bone fractures. The lower plasma folate level is reported in the AA genotype of the rs2241777 SNP in the 3'UTR region (Urano et al. 2014). This study demonstrates that gene variants in the mitochondrial folate transporter SLC25A32 can impact folate metabolism such that lower concentrations are associated with increased risk for skeletal disorders. Clearly, interfering with folate transport can have significant impacts on embryonic development and human disease states. Our study is based on the association with between *SLC25A32* polymorphism and folate 1C metabolism regulation and suggests that inactivation of *Slc25a32* gene is able to impair the mitochondrial folate-mediated 1C metabolism and results in NTDs in mouse.

Previous investigations have demonstrated that the mitochondrial folate transporter encoded by the *Slc25a32* gene is located in the inner mitochondrial membrane and recognizes THF in mammalian systems (Lawrence et al. 2011) (Titus & Moran 2000). In the mitochondria, folate 1C metabolism involves transferring 1C units from donors (Serine,

glycine, and formate) to an acceptor (THF). An adequate amount of THF is essential for progression of mitochondrial folate 1C catabolism, and the production of formate is required for the *de novo* synthesis of purines and thymidylate in the cytosol (Tibbetts & Appling 2010). Several studies have shown that inactivation of folate 1C enzymes leads to an increased risk of NTDs as well as embryonic growth retardation. In transgenic mouse models lacking functional *AMT* and *Mthfd1l* genes, which encode enzymes involved in mitochondrial folate 1C metabolism, NTDs are frequent developmental outcomes. Aminomethyltransferase (*AMT*) is one of the GCS components in mitochondria (Narisawa et al. 2012). The GCS plays a critical role in mitochondrial folate metabolism by providing 1C units from glycine to THF, thereby generating CH_2-THF. Those fetuses lacking *AMT* had NTDs, confirming the linkage between mitochondrial folate mediated 1C metabolism via the GCS, and its deleterious impact on NTC during early embryonic development (Narisawa et al. 2012). The *Mthfd1l* is an monodirectional enzyme that generates formate from 10-formyl-THF in the mitochondria to support the cytoplasmic nucleotide biosynthesis (Tibbetts & Appling 2010). The *Mthfd1l* knockout embryos exhibited NTDs including exencephaly and craniorachischisis with a wavy neural tube, and a high prevalence of embryonic lethality (Momb et al. 2013). In the present study, embryos lacking a functional *Slc25a32* gene always had an NTD, either exencephaly or craniorachischisis, often resulting in embryonic lethality as well, showing the consistent neural tube phenotypes with other mouse models that impact mitochondrial 1C metabolism.

By contrast, inactivation of the cytosolic folate 1C enzymes, *Mthfr* and *Mthfd1*, does not result in an increased risk for NTDs in the mouse (Copp, Stanier, and Greene 2013). The enzyme MTHFR encoded by the *MTHFR* gene is responsible for reduction of CH_3-THF for the cytosolic methyl cycle (Tibbetts & Appling 2010). The C677T polymorphism of *MTHFR* is linked with NTDs in human (Kirke 2004), while the deletion of *Mthfr* gene in mice resulted in pups who exhibited growth retardation and abnormal lipid deposition (Chen et al. 2001), yet failed to express NTDs even among the progeny of maternal *Mthfr* deficient dams maintained on a low folate diet (Li et al. 2005). The enzyme MTHFD1, encoded by the *MTHFD1* gene is a trifunctional C1-THF synthase required for nucleotide biosynthesis in the cytosol (Tibbetts & Appling 2010). The transgenic $Mthfdl^{gt/gt}$ embryos often died *in utero*, demonstrating that *Mthfd1* gene is essential for murine development. $Mthfd1^{gt/+}$ dams maintained on a low folate diet produced progeny suffering from fetal growth inhibition, although these wild-type and heterozygous offspring did not present with NTDs (Beaudin, Perry, et al. 2012). Taken together, these studies suggest that inactivation of mitochondrial 1C metabolism has a more severe impact on NTC resulting in a very high prevalence of NTDs relative to the many cytoplasmic 1C metabolism enzymes that have been knocked out in mutant mice.

Inactivation of cytosolic enzyme *Shmt1* that is required for thymidylate biosynthesis and homocysteine remethylation also results in NTD affected embryos in the mouse model. The $Shmt1^{-/-}$ embryos displayed exencephaly when the dam was stressed by a folate deficient diet, whereas NTDs were not observed when the dams were maintained on a folate replete diet (Beaudin, Abarinov, et al. 2012). The $Slc25a32^{gt/gt}$ embryos have an

NTD phenotype in spite of the dams being maintained on a standard rodent chow containing 3 ppm of FA. Indeed, maternal folate supplementation (5-mTHF) of *Slc25a32*$^{+/gt}$ dams has no beneficial effect in terms of rescuing the normal phenotype in *Slc25a32*$^{gt/gt}$ embryos (Table 3). This is consistent with previously reported results that maternal folic acid supplementation was ineffective in reducing the prevalence of NTDs in both *AMT*$^{-/-}$ and *Mthfd1l*$^{z/z}$ embryos (Momb & Appling 2014).

We observed that maternal calcium formate supplementation of the *Slc25a32*$^{+/gt}$ dam partially rescues the NTDs in the *Slc25a32*$^{gt/gt}$ embryos (Fig. 8). Similarly, maternal sodium formate supplementation of *Mthfd1l*$^{z/+}$ dams significantly reduced the incidence of NTDs in the *Mthfd1l* null embryos, demonstrating that the mitochondrial folate 1C metabolism is strongly linked with NTD incidence (Momb et al. 2013). The formate is derived from the mitochondrial folate 1C metabolism and the formate status of the embryo influences the failure of NTC. This impact appears due to altered *de novo* purine and pyrimidine synthesis that is essential for DNA replication and required during cell proliferation (Tibbetts & Appling 2010). In addition, previous studies have shown that disruption of purine and thymidylate biosynthesis gives rise to NTD in the mouse, demonstrating the importance of purine and thymidylate in NTC (Beaudin et al. 2011) (Fleming & Copp 1998). Thus, the rescue of NTDs in the *Slc25a32* deficient mouse in response to calcium formate supplementation is consistent with the notion that disruption of the mitochondrial folate 1C metabolism leads to an increased risk of NTDs. Given the mitochondrial nature of the *Mthfd1l* and *Slc25a32* genes, it is not surprising that FA

supplementation failed to rescue the phenotype, while exogenous concentrations of the calcium formate did provide partial rescue.

Previous studies have demonstrated that normal mitochondrial function is associated with proper folate 1C metabolism. The function of mitochondria is to provide ATP production of energy metabolism, mitochondrial respiration, and contribute to glycine metabolism. In human cells, mitochondrial respiratory chain dysfunction leads to the impairment of the mitochondrial 1C metabolic pathway, demonstrating that inhibition of mitochondrial respiratory chain triggered aberrant of serine metabolism (Bao et al. 2016). Irregularity of 1C metabolism was linked with mitochondrial DNA (mtDNA) hypermethylation resulting in mitochondrial malfunction and leading to impaired nucleotide metabolism secondary to mtDNA genomic instability (Desler et al. 2010) (Jia et al. 2016). Given that abnormal 1C metabolism could contribute to mitochondrial dysfunction, it is possible that lacking a functional *Slc25a32* gene increases the risk for NTDs in response to either 1C metabolism or mitochondrial dysfunction due to mitochondrial THF deficiency.

Transcriptomic analysis of *Slc25a32* embryos identified multiple transcription factors and signaling pathways that are critical to the cellular and molecular mechanisms involved during normal neural tube development (Table 8-9 and Fig. 12-13). Several studies have determined that interaction between transcription factors and signaling pathway regulate the morphological movements of neuroepithelial cells, and if aberrant, can lead to NTDs (Nikolopoulou et al. 2017). Previously, the transcription factor *Pax3* was shown to be critical to successful NTC, as inactivating this gene produced embryos with

exencephaly (Epstein, Vekemans, and Gros 1991). The *Lhx2-Lhx9* deficient zebrafish embryos had differentiation defects of thalamic neurons, suggesting that the transcription factors *Lhx2* and *Lhx9* are essential for the development of the caudal forebrain (Peukert et al. 2011). Additionally, the *Cdx* genes encode homeodomain transcription factors, and *Cdx1-Cdx2* double knockout mutants exhibit a severe form of craniorachischisis. These *Cdx* genes impact NTC by altering the regulation of the planar cell polarity (PCP) signaling-related gene *Ptk7* (Savory et al. 2011). PCP signaling is one of the key pathways involved during early neural tube development, with the role of regulating polarized cellular motility of epithelia in a morphogenetic process known as convergent extension (Nikolopoulou et al. 2017). The *Slc25a32* knockout embryos frequently present with a remarkably similar phenotype involving craniorachischisis, and their RNA-seq data clearly indicates the down-regulation of the PCP signaling pathway. Indeed, the RNA-seq data of *Slc25a32* null embryos show an up-regulation of Rho family GTPase and RhoA signaling pathway, well-known key signaling pathways involved in NTC (Fig. 13). Activation of Rho and Rho-kinase is essential for establishing the shape of the neural plate under apical accumulation in neuroepithelial cells (Kinoshita et al. 2008). Taken together, these results demonstrate that perturbation of the *Slc25a32* gene induces a severe NTD phenotype, secondary to dysregulated signaling in the PCP, Rho family GTPase, and RhoA signaling pathways which interfere with normal NTC. In gene ontology enrichment, several genes were identified in dysregulated biological process including muscle tissue development, and regulation of cell morphogenesis including cell-cell junctions in the apical portions of the cell (Fig. 11), suggesting the aberrant cellular behavior associated with morphogenetic

processes during NTC (Greene & Copp 2014). The RNA-seq data identified several dysregulated folate 1C metabolism genes including *Fpgs*, *Mthfs*, *Dhfr* and *Mthfd2l* (Table 7), further demonstrating the importance of proper regulation of the folate 1C metabolism to proper closure of the neural tube, and how the lack of essential mitochondrial folate transport in *Slc25a32* nullizygous embryos contribute to their 100% prevalent NTDs.

In closing, we generated and characterized a novel *Slc25a32* knockout mouse model that demonstrates the importance of a mitochondrial folate transporter in neural tube development. The disruption of the *Slc25a32* gene in the mouse results either in fully penetrant NTDs, or in embryo-fetal lethality. These results from this study lead us to conclude that mitochondrial folate 1C metabolism plays a critical role in promoting normal NTC. We believe that a better understanding of the critically important role of mitochondrial FA transport and metabolism in NTD susceptibility will help explain the beneficial effect that 1C donors have on embryonic development, and provide a pathway for developing novel interventions for non-folate responsive NTDs.

5 References

Abdul-Aziz, Noraishah M., Mark Turmaine, Nicholas D E Greene, and Andrew J. Copp. 2009. "EphrinA-EphA Receptor Interactions in Mouse Spinal Neurulation: Implications for Neural Fold Fusion." *International Journal of Developmental Biology* 53 (4): 559–68. doi:10.1387/ijdb.082777na.

Agrimi, G, M A Di Noia, C M Marobbio, G Fiermonte, F M Lasorsa, and F Palmieri. 2004. "Identification of the Human Mitochondrial S-Adenosylmethionine Transporter: Bacterial Expression, Reconstitution, Functional Characterization and Tissue Distribution." *Biochem J* 379 (Pt 1): 183–90. doi:10.1042/bj20031664.

Bao, Xiaoyan Robert, Shao-en Ong, Olga Goldberger, Jun Peng, Rohit Sharma, Dawn A Thompson, Scott B Vafai, et al. 2016. "Mitochondrial Dysfunction Remodels One-Carbon Metabolism in Human Cells." *eLife*, 1–24. doi:10.7554/eLife.10575.

Barlowe, C K, and D R Appling. 1988a. "In Vitro Evidence for the Involvement of Mitochondrial Folate Metabolism in the Supply of Cytoplasmic One-Carbon Units." *BioFactors (Oxford, England)* 1 (2): 171–76. doi:2475123.

———. 1988b. "In Vitro Evidence for the Involvement of Mitochondrial Folate Metabolism in the Supply of Cytoplasmic One-Carbon Units." *BioFactors (Oxford, England)* 1 (2): 171–76. doi:2475123.

Beaudin, Anna E., Elena V. Abarinov, Olga Malysheva, Cheryll A. Perry, Marie Caudill, and Patrick J. Stover. 2012. "Dietary Folate, but Not Choline, Modifies Neural Tube Defect Risk in Shmt1 Knockout Mice." *American Journal of Clinical Nutrition* 95 (1): 109–14. doi:10.3945/ajcn.111.020305.

Beaudin, Anna E., Elena V. Abarinov, Drew M. Noden, Cheryll A. Perry, Stephanie Chu, Sally P. Stabler, Robert H. Allen, and Patrick J. Stover. 2011. "Shmt1 and de Novo Thymidylate Biosynthesis Underlie Folate-Responsive Neural Tube Defects in Mice." *American Journal of Clinical Nutrition* 93 (4): 789–98. doi:10.3945/ajcn.110.002766.

Beaudin, Anna E., Cheryll A. Perry, Sally P. Stabler, Robert H. Allen, and Patrick J. Stover. 2012. "Maternal Mthfd1 Disruption Impairs Fetal Growth but Does Not Cause Neural Tube Defects in Mice." *American Journal of Clinical Nutrition* 95 (4): 882–91. doi:10.3945/ajcn.111.030783.

Boutin, C., O. Hardt, A. de Chevigny, N. Core, S. Goebbels, R. Seidenfaden, A. Bosio, and H. Cremer. 2010. "NeuroD1 Induces Terminal Neuronal Differentiation in Olfactory Neurogenesis." *Proceedings of the National Academy of Sciences* 107 (3): 1201–6. doi:10.1073/pnas.0909015107.

Carrel, T, S M Purandare, W Harrison, F Elder, T Fox, B Casey, and G E Herman. 2000. "The X-Linked Mouse Mutation Bent Tail Is Associated with a Deletion of the Zic3 Locus." *Human Molecular Genetics* 9 (13): 1937–42.

Centers for Disease Control and Prevention (CDC). 2004. “Spina Bifida and Anencephaly before and after Folic Acid Mandate--United States, 1995-1996 and 1999-2000.” *MMWR. Morbidity and Mortality Weekly Report* 53 (17): 362–65. doi:10.1001/jama.292.3.325.

Chen, Z., a C Karaplis, S L Ackerman, I P Pogribny, S Melnyk, S Lussier-Cacan, M F Chen, et al. 2001. “Mice Deficient in Methylenetetrahydrofolate Reductase Exhibit Hyperhomocysteinemia and Decreased Methylation Capacity, with Neuropathology and Aortic Lipid Deposition.” *Human Molecular Genetics* 10 (5): 433–43. doi:10.1093/hmg/10.5.433.

Chu, Edward, and Carmen J. Allegra. 1996. “The Role of Thymidylate Synthase in Cellular Regulation.” In *Advances in Enzyme Regulation*, 36:143–63. doi:10.1016/0065-2571(95)00004-6.

Cooley, Marion A., Christine B. Kern, Victor M. Fresco, Andy Wessels, Robert P. Thompson, Tim C. McQuinn, Waleed O. Twal, Corey H. Mjaatvedt, Christopher J. Drake, and W. Scott Argraves. 2008. “Fibulin-1 Is Required for Morphogenesis of Neural Crest-Derived Structures.” *Developmental Biology* 319 (2): 336–45. doi:10.1016/j.ydbio.2008.04.029.

Copp, Andrew J, and Nicholas D E Greene. 2012. “Neural Tube Defects--Disorders of Neurulation and Related Embryonic Processes.” *Wiley Interdisciplinary Reviews. Developmental Biology* 2 (2): 213–27. doi:10.1002/wdev.71.

Copp, Andrew J, Philip Stanier, and Nicholas D E Greene. 2013. “Neural Tube Defects: Recent Advances, Unsolved Questions, and Controversies.” *The Lancet. Neurology* 12 (8): 799–810. doi:10.1016/S1474-4422(13)70110-8.

Crider, K. S., T. P. Yang, R. J. Berry, and L. B. Bailey. 2012. “Folate and DNA Methylation: A Review of Molecular Mechanisms and the Evidence for Folate’s Role.” *Advances in Nutrition: An International Review Journal* 3 (1): 21–38. doi:10.3945/an.111.000992.

Cybulski, R L, and R R Fisher. 1977. “Mitochondrial Neutral Amino Acid Transport: Evidence for a Carrier Mediated Mechanism.” *Biochemistry* 16 (23): 5116–20.

Czeizel, Andrew E. 1998. “Periconceptional Folic Acid Containing Multivitamin Supplementation.” In *European Journal of Obstetrics Gynecology and Reproductive Biology*, 78:151–61. doi:10.1016/S0301-2115(98)00061-X.

Desler, Claus, Anne Lykke, and Lene Juel Rasmussen. 2010. “The Effect of Mitochondrial Dysfunction on Cytosolic Nucleotide Metabolism” 2010. doi:10.4061/2010/701518.

Ducker, Gregory S., and Joshua D. Rabinowitz. 2016. “One-Carbon Metabolism in Health and Disease.” *Cell Metabolism*, no. 2016. Elsevier Inc.: 1–16. doi:10.1016/j.cmet.2016.08.009.

Epstein, Douglas J., Michel Vekemans, and Philippe Gros. 1991. "Splotch (Sp2H), a Mutation Affecting Development of the Mouse Neural Tube, Shows a Deletion within the Paired Homeodomain of Pax-3." *Cell* 67 (4): 767–74. doi:10.1016/0092-8674(91)90071-6.

Fleming, a, and a J Copp. 1998. "Embryonic Folate Metabolism and Mouse Neural Tube Defects." *Science (New York, N.Y.)* 280 (1998): 2107–9. doi:10.1126/science.280.5372.2107.

García-Martínez, L F, and D R Appling. 1993. "Characterization of the Folate-Dependent Mitochondrial Oxidation of Carbon 3 of Serine." *Biochemistry* 32 (17): 4671–76. http://www.ncbi.nlm.nih.gov/pubmed/8485144.

Greene, Nicholas D E, and Andrew J Copp. 2014. "Neural Tube Defects." *Annu Rev Neurosci* 37: 221–42. doi:10.1146/annurev-neuro-062012-170354.Neural.

Hampson, Robert K, Melanie K Taylor, and Merle S Olson. 1983. "Regulation of the Glycine Cleavage System in the Isolated Rat Liver Mitochondria" 258: 2993–99.

Ho, Vikki, Thomas E Massey, and Will D King. 2013. "Effects of Methionine Synthase and Methylenetetrahydrofolate Reductase Gene Polymorphisms on Markers of One-Carbon Metabolism." *Genes & Nutrition* 8 (6): 571–80. doi:10.1007/s12263-013-0358-2.

Jia, Longfei, Juan Li, Bin He, Yimin Jia, Yingjie Niu, Chenfei Wang, and Ruqian Zhao. 2016. "Abnormally Activated One-Carbon Metabolic Pathway Is Associated with mtDNA Hypermethylation and Mitochondrial Malfunction in the Oocytes of Polycystic Gilt Ovaries." *Nature Publishing Group*, no. January. Nature Publishing Group: 1–11. doi:10.1038/srep19436.

Kao, F, L Chasin, and T T Puck. 1969. "Genetics of Somatic Mammalian Cells. X. Complementation Analysis of Glycine-Requiring Mutants." *Proceedings of the National Academy of Sciences of the United States of America* 64 (4): 1284–91. doi:10.1073/pnas.64.4.1284.

Kikuchi, Goro, Yutaro Motokawa, Tadashi Yoshida, and Koichi Hiraga. 2008. "Glycine Cleavage System: Reaction Mechanism, Physiological Significance, and Hyperglycinemia." *Proceedings of the Japan Academy. Series B, Physical and Biological Sciences* 84 (7): 246–63. doi:10.2183/pjab.84.246.

Kinoshita, Nagatoki, Noriaki Sasai, Kazuyo Misaki, and Shigenobu Yonemura. 2008. "Apical Accumulation of Rho in the Neural Plate Is Important for Neural Plate Cell Shape Change and Neural Tube Formation." *Molecular Biology of the Cell* 19 (5): 2289–99. doi:10.1091/mbc.E07-12-1286.

Kirke, P. N. 2004. "Impact of the MTHFR C677T Polymorphism on Risk of Neural Tube Defects: Case-Control Study." *Bmj* 328 (7455): 1535–36. doi:10.1136/bmj.38036.646030.EE.

Lamers, Yvonne, Jerry Williamson, Douglas W Theriaque, Jonathan J Shuster, Lesa R Gilbert, Christine Keeling, Peter W Stacpoole, and Jesse F Gregory Iii. 2009. "Production of 1-Carbon Units from Glycine Is Extensive in Healthy Men and Women 1,2." *J. Nutr* 139: 666–71. doi:10.3945/jn.108.103580.

Lane, Andrew N., and Teresa W M Fan. 2015. "Regulation of Mammalian Nucleotide Metabolism and Biosynthesis." *Nucleic Acids Research*. doi:10.1093/nar/gkv047.

Lawrence, Scott a, John C Hackett, and Richard G Moran. 2011. "Tetrahydrofolate Recognition by the Mitochondrial Folate Transporter." *The Journal of Biological Chemistry* 286 (36): 31480–89. doi:10.1074/jbc.M111.272187.

Li, Deqiang, Laura Pickell, Ying Liu, Qing Wu, Jeffrey S Cohn, and Rima Rozen. 2005. "Maternal Methylenetetrahydrofolate Reductase Deficiency and Low Dietary Folate Lead to Adverse Reproductive Outcomes and Congenital Heart Defects in Mice." *American Society for Clinical Nutrition* 82 (1): 188–95.

Lucock, M. 2000. "Folic Acid: Nutritional Biochemistry, Molecular Biology, and Role in Disease Processes." *Molecular Genetics and Metabolism* 71 (1–2): 121–38. doi:10.1006/mgme.2000.3027.

MacFarlane, Amanda J., Cheryll A. Perry, Hussein H. Girnary, Dacao Gao, Robert H. Allen, Sally P. Stabler, Barry Shane, and Patrick J. Stover. 2009. "Mthfd1 Is an Essential Gene in Mice and Alters Biomarkers of Impaired One-Carbon Metabolism." *Journal of Biological Chemistry* 284 (3): 1533–39. doi:10.1074/jbc.M808281200.

Mejia, Narciso R., and Robert E. MacKenzie. 1988. "NAD-Dependent Methylenetetrahydrofolate Dehydrogenase-Methenyltetrahydrofolate Cyclohydrolase in Transformed Cells Is a Mitochondrial Enzyme." *Biochemical and Biophysical Research Communications* 155 (1): 1–6. doi:10.1016/S0006-291X(88)81040-4.

Mitchell, Laura E. 2005. "Epidemiology of Neural Tube Defects." *American Journal of Medical Genetics. Part C, Seminars in Medical Genetics* 135C (1): 88–94. doi:10.1002/ajmg.c.30057.

Momb, Jessica, and Dean R Appling. 2014. "Mitochondrial One-Carbon Metabolism and Neural Tube Defects." *Birth Defects Research. Part A, Clinical and Molecular Teratology*. doi:10.1002/bdra.23268.

Momb, Jessica, Jordan P Lewandowski, Joshua D Bryant, Rebecca Fitch, Deborah R Surman, Steven a Vokes, and Dean R Appling. 2013. "Deletion of Mthfd1l Causes Embryonic Lethality and Neural Tube and Craniofacial Defects in Mice." *Proceedings of the National Academy of Sciences of the United States of America* 110 (2): 549–54. doi:10.1073/pnas.1211199110.

MRC VITAMIN STUDY RESEARCH GROUP. 1991. “Prevention of Neural Tube Defects: Results of the Medical Research Council Vitamin Study.” *The Lancet* 338 (8760): 131–37. doi:10.1016/0140-6736(91)90133-A.

Murray, Christopher J L, Alan D Lopez, Harvard School of Public Health., World Health Organization., and World Bank. 1998. *Health Dimensions of Sex and Reproduction : The Global Burden of Sexually Transmitted Diseases, HIV, Maternal Conditions, Perinatal Disorders, and Congenital Anomalies*. *Global Burden of Disease and Injury Series ;*

Narisawa, Ayumi, Shoko Komatsuzaki, Atsuo Kikuchi, Tetsuya Niihori, Yoko Aoki, Kazuko Fujiwara, Mitsuyo Tanemura, et al. 2012. “Mutations in Genes Encoding the Glycine Cleavage System Predispose to Neural Tube Defects in Mice and Humans.” *Human Molecular Genetics* 21 (7): 1496–1503. doi:10.1093/hmg/ddr585.

Nikolopoulou, Evanthia, Gabriel L. Galea, Ana Rolo, Nicholas D. E. Greene, and Andrew J. Copp. 2017. “Neural Tube Closure: Cellular, Molecular and Biomechanical Mechanisms.” *Development* 144 (4): 552–66. doi:10.1242/dev.145904.

Nishimura, Tamako, Hisao Honda, and Masatoshi Takeichi. 2012. “Planar Cell Polarity Links Axes of Spatial Dynamics in Neural-Tube Closure.” *Cell* 149 (5): 1084–97. doi:10.1016/j.cell.2012.04.021.

Palmieri, Ferdinando. 2013. “The Mitochondrial Transporter Family SLC25: Identification, Properties and Physiopathology.” *Molecular Aspects of Medicine*. doi:10.1016/j.mam.2012.05.005.

Peukert, Daniela, Sabrina Weber, Andrew Lumsden, and Steffen Scholpp. 2011. “Lhx2 and Lhx9 Determine Neuronal Differentiation and Compartition in the Caudal Forebrain by Regulating Wnt Signaling.” *PLoS Biology* 9 (12). doi:10.1371/journal.pbio.1001218.

Pfendner, Walter, and Lewis I. Pizer. 1980. “The Metabolism of Serine and Glycine in Mutant Lines of Chinese Hamster Ovary Cells.” *Archives of Biochemistry and Biophysics* 200 (2): 503–12. doi:10.1016/0003-9861(80)90382-3.

Piedrahita, J a, B Oetama, G D Bennett, J van Waes, B a Kamen, J Richardson, S W Lacey, R G Anderson, and R H Finnell. 1999. “Mice Lacking the Folic Acid-Binding Protein Folbp1 Are Defective in Early Embryonic Development.” *Nature Genetics* 23 (october): 228–32. doi:10.1038/13861.

Pike, Schuyler T., Rashmi Rajendra, Karen Artzt, and Dean R. Appling. 2010. “Mitochondrial C1-Tetrahydrofolate Synthase (MTHFD1L) Supports the Flow of Mitochondrial One-Carbon Units into the Methyl Cycle in Embryos.” *Journal of Biological Chemistry* 285 (7): 4612–20. doi:10.1074/jbc.M109.079855.

Prasannan, Priya, and Dean R. Appling. 2009. “Human Mitochondrial C1-Tetrahydrofolate Synthase: Submitochondrial Localization of the Full-Length Enzyme and

Characterization of a Short Isoform." *Archives of Biochemistry and Biophysics* 481 (1): 86–93. doi:10.1016/j.abb.2008.10.028.

Prasannan, Priya, Schuyler Pike, Kun Peng, Barry Shane, and Dean R. Appling. 2003. "Human Mitochondrial C1-Tetrahydrofolate Synthase: Gene Structure, Tissue Distribution of the mRNA, and Immunolocalization in Chinese Hamster Ovary Cell." *Journal of Biological Chemistry* 278 (44): 43178–87. doi:10.1074/jbc.M304319200.

Saitsu, Hirotomo. 2017. "Folate Receptors and Neural Tube Closure." *Congenital Anomalies* 1: 1–4. doi:10.1111/cga.12218.

Salojin, Konstantin V., Robert M. Cabrera, Weimei Sun, Wei Chun Chang, Colin Lin, Lindsay Duncan, Ken A. Platt, et al. 2011. "A Mouse Model of Hereditary Folate Malabsorption: Deletion of the PCFT Gene Leads to Systemic Folate Deficiency." *Blood* 117 (18): 4895–4904. doi:10.1182/blood-2010-04-279653.

Savory, Joanne G. A., Melissa Mansfield, Filippo M. Rijli, and David Lohnes. 2011. "Cdx Mediates Neural Tube Closure through Transcriptional Regulation of the Planar Cell Polarity Gene *Ptk7*." *Development* 138 (7): 1361–70. doi:10.1242/dev.056622.

Shin, Minhye, Joshua D. Bryant, Jessica Momb, and Dean R. Appling. 2014. "Mitochondrial MTHFD2L Is a Dual Redox Cofactor-Specific Methylenetetrahydrofolate Dehydrogenase/methenyltetrahydrofolate Cyclohydrolase Expressed in Both Adult and Embryonic Tissues." *Journal of Biological Chemistry* 289 (22): 15507–17. doi:10.1074/jbc.M114.555573.

Tibbetts, Anne S., and Dean R. Appling. 2010. "Compartmentalization of Mammalian Folate-Mediated One-Carbon Metabolism." *Annual Review of Nutrition* 30 (1): 57–81. doi:10.1146/annurev.nutr.012809.104810.

Titus, S a, and R G Moran. 2000. "Retrovirally Mediated Complementation of the glyB Phenotype. Cloning of a Human Gene Encoding the Carrier for Entry of Folates into Mitochondria." *The Journal of Biological Chemistry* 275 (47): 36811–17. doi:10.1074/jbc.M005163200.

Urano, Tomohiko, Masataka Shiraki, Mitsuru Saito, Noriko Sasaki, Yasuyoshi Ouchi, and Satoshi Inoue. 2014. "Polymorphism of SLC25A32 , the Folate Transporter Gene, Is Associated with Plasma Folate Levels and Bone Fractures in Japanese Postmenopausal Women." *Geriatrics & Gerontology International* 14 (4): 942–46. doi:10.1111/ggi.12201.

Waes, Janee Gelineau Van, Steven Heller, Linda K. Bauer, Justin Wilberding, Joyce R. Maddox, Francisco Aleman, Thomas H. Rosenquist, and Richard H. Finnell. 2008. "Embryonic Development in the Reduced Folate Carrier Knockout Mouse Is Modulated by Maternal Folate Supplementation." *Birth Defects Research Part A - Clinical and Molecular Teratology* 82 (7): 494–507. doi:10.1002/bdra.20453.

Wu, Gang, Xupei Huang, Yimin Hua, and Dezhi Mu. 2011. “Roles of Planar Cell Polarity Pathways in the Development of Neural [Correction of Neutral] Tube Defects.” *Journal of Biomedical Science* 18 (1): 66. doi:10.1186/1423-0127-18-66.

Ybot-Gonzalez, P., C. Gaston-Massuet, G. Girdler, J. Klingensmith, R. Arkell, N. D. E. Greene, and A. J. Copp. 2007. “Neural Plate Morphogenesis during Mouse Neurulation Is Regulated by Antagonism of Bmp Signalling.” *Development* 134 (17): 3203–11. doi:10.1242/dev.008177.

Yoshida, Tadashi, and Goro Kikuchi. 1970. “Major Pathways of Glycine and Serine Catabolism in Rat Liver.” *Archives of Biochemistry and Biophysics* 139 (2): 380–92. doi:10.1016/0003-9861(70)90490-X.